MINISTÉRIO DA CIÊNCIA, TECNOLOGIA E INOVAÇÃO
INSTITUTO NACIONAL DE PESQUISAS ESPACIAIS

sid.inpe.br/mtc-m21d/2024/02.08.16.33-TDI

THE INFLUENCE OF SHORTWAVE SOLAR RADIATION ON LIGHTNING ACTIVITY IN THE METROPOLITAN REGION OF SÃO PAULO: THE WHITEHOUSE EFFECT

Abdala Elias Nader

Master's Dissertation of the Graduate Course in Space Geophysics, guided by Dr. Kleber Pinheiro Naccarato, approved in December 15, 2023.

URL of the original document:
<http://urlib.net/8JMKD3MGP3W34T/4AMQJKL>

INPE
São José dos Campos
2023

PUBLISHED BY:

Instituto Nacional de Pesquisas Espaciais - INPE
Coordenação de Ensino, Pesquisa e Extensão (COEPE)
Divisão de Biblioteca (DIBIB)
CEP 12.227-010
São José dos Campos - SP - Brasil
Tel.:(012) 3208-6923/7348
E-mail: pubtc@inpe.br

MINISTÉRIO DA CIÊNCIA, TECNOLOGIA E INOVAÇÃO
INSTITUTO NACIONAL DE PESQUISAS ESPACIAIS

sid.inpe.br/mtc-m21d/2024/02.08.16.33-TDI

THE INFLUENCE OF SHORTWAVE SOLAR RADIATION ON LIGHTNING ACTIVITY IN THE METROPOLITAN REGION OF SÃO PAULO: THE WHITEHOUSE EFFECT

Abdala Elias Nader

Master's Dissertation of the Graduate Course in Space Geophysics, guided by Dr. Kleber Pinheiro Naccarato, approved in December 15, 2023.

URL of the original document:
<http://urlib.net/8JMKD3MGP3W34T/4AMQJKL>

INPE
São José dos Campos
2023

Cataloging in Publication Data

Nader, Abdala Elias.

N125i The influence of shortwave solar radiation on lightning activity in the metropolitan region of São Paulo: the whitehouse effect / Abdala Elias Nader. – São José dos Campos : INPE, 2023.

xxiv + 64 p. ; (sid.inpe.br/mtc-m21d/2024/02.08.16.33-TDI)

Dissertation (Master in Space Geophysics) – Instituto Nacional de Pesquisas Espaciais, São José dos Campos, 2023.

Guiding : Dr. Kleber Pinheiro Naccarato.

1. Boomerang effect. 2. whitehouse effect. 3. shortwave radiation. 4. Metropolitan region of São Paulo. 5. Lightning activity. I.Title.

CDU 551.521.32(815.6)

MINISTÉRIO DA CIÊNCIA, TECNOLOGIA E INOVAÇÃO

INSTITUTO NACIONAL DE PESQUISAS ESPACIAIS
Serviço de Pós-Graduação - SEPGR

DEFESA FINAL DE DISSERTAÇÃO DE ABDALA ELIAS NADER
REG. 365881/2021, BANCA Nº 304/2023

No dia 15 de dezembro de 2023, presencialmente no Auditório CEA II, o(a) aluno(a) mencionado(a) acima defendeu seu trabalho final (apresentação oral seguida de arguição) perante uma Banca Examinadora, cujos membros estão listados abaixo. O(A) aluno(a) foi APROVADO(A) pela Banca Examinadora, por unanimidade, em cumprimento ao requisito exigido para obtenção do Título de Mestre em Geofísica Espacial / Ciências Atmosféricas, com a exigência de que o trabalho final a ser publicado deverá incorporar as correções sugeridas pela Banca Examinadora, com revisão pelo(s) orientador(es).

Novo Título: The influence of shortwave solar radiation on lightning activity in the Metropolitan Region of São Paulo: the whitehouse effect

Membros da banca:

Dr. Plínio Carlos Alvalá – Presidente – INPE
Dr. Kleber Pinheiro Naccarato – Orientador – INPE
Dr. Marcelo Magalhães Fares Saba – Membro Interno – INPE
Dra. Simone Marilene Sievert Da Costa Coelho – Membro Interno – INPE
Dr. Antonio Carlos Varela Saraiva - Membro Externo - UNESP

Documento assinado eletronicamente por **Kleber Pinheiro Naccarato**, **Pesquisador**, em 20/12/2023, às 10:39 (horário oficial de Brasília), com fundamento no § 3º do art. 4º do Decreto nº 10.543, de 13 de novembro de 2020.

Documento assinado eletronicamente por **Marcelo Magalhães Fares Saba**, **Pesquisador**, em 20/12/2023, às 10:40 (horário oficial de Brasília), com fundamento no § 3º do art. 4º do Decreto nº 10.543, de 13 de novembro de 2020.

Documento assinado eletronicamente por **Plinio Carlos Alvala**, **Pesquisador Titular**, em 20/12/2023, às 10:41 (horário oficial de Brasília), com fundamento no § 3º do art. 4º do Decreto nº 10.543, de 13 de novembro de 2020.

Documento assinado eletronicamente por **Simone Marilene Sievert da Costa Coelho**, **Pesquisadora**, em 20/12/2023, às 10:47 (horário oficial de Brasília), com fundamento no § 3º do art. 4º do Decreto nº 10.543, de 13 de novembro de 2020.

Documento assinado eletronicamente por **Antonio carlos varela saraiva (E)**, **Usuário Externo**, em 20/12/2023, às 11:42 (horário oficial de Brasília), com fundamento no § 3º do art. 4º do Decreto nº 10.543, de 13 de novembro de 2020.

A autenticidade deste documento pode ser conferida no site https://sei.mcti.gov.br/verifica.html, informando o código verificador **11591440** e o código CRC **3E74E01A**.

Referência: Processo nº 01340.010393/2023-76 SEI nº 11591440

To Esther, my beloved.

For all the joy in the happiest moments and for all the help in the most difficult times.

SPECIAL THANKS

To my parents, who despite all the difficulties, trusted me ever since I decided to be a scientist.

To my father, who taught me the value and importance of knowledge.

My mother, who always helped me face my fears.

To Esther, my beloved, who always told me that everything will be fine.

To my friends, my dear brothers, who are part of the funniest moments of my life.

A special thank you to all the adventure writers I read in my childhood who inspired me to seek to know and discover the mysteries of the world and science, especially Jules Verne, Herman Melville and Jonathan Swift.

To my advisor, Prof. Dr. Kleber Pinheiro Naccarato, who I greatly admire as a scientist and person. That has always given me confidence and makes me believe in my work.

The Prof. Dr. Simone Sievert, who followed the work closely, helping with lots of information and guiding the best path forward.

To Helmut Muniz, who always promptly provided his assistance in collecting radiation data.

To the members of the examining board, who brought suggestions that enriched the work.

To Conselho Nacional de Desenvolvimento Científico e Tecnológico (CNPq), in English (National Council for Scientific and Technological Development), for the financial support of this work.

To Fundação Coordenação de Aperfeiçoamento de Pessoal de Nível Superior (CAPES), for financial support during part of this work.

AGRADECIMENTOS (IN PORTUGUESE)

A meus pais, que mesmo com todas as dificuldades confiaram em mim desde quando decidi ser um cientista.

A meu pai, que me ensinou o valor e a importância do conhecimento.

A minha mãe, que sempre me ajudou a enfrentar meus medos.

A Esther, minha amada, que sempre me disse que tudo ficará bem.

Aos meus amigos, meus queridos irmãos, que fazem parte dos momentos mais engraçados da minha vida.

Um agradecimento especial a todos os escritores de aventuras que li na minha infância que me inspiraram a buscar conhecer e descobrir os mistérios do mundo e a ciência, especialmente Jules Verne, Herman Melville e Jonathan Swift.

Ao meu orientador, Prof. Dr. Kleber Pinheiro Naccarato, que eu admiro muito como cientista e pessoa. Que sempre me deu confiança e me faz acreditar no meu trabalho.

A Profa. Dra. Simone Sievert, que acompanhou de perto os trabalhos, ajudando com muitas informações e orientando os melhores caminhos a seguir.

Ao Helmut Muniz, que sempre com celeridade forneceu sua ajuda na coleta de dados de radiação.

Aos membros da banca examinadora, que trouxeram sugestões que enriqueceram o trabalho.

Ao Conselho Nacional de Desenvolvimento Científico e Tecnológico (CNPq), pelo suporte financeiro deste trabalho.

A Fundação Coordenação de Aperfeiçoamento de Pessoal de Nível Superior (CAPES) pelo suporte financeiro durante uma parte deste trabalho.

"…Consider all this; and then turn to this green, gentle, and most docile earth; consider them both, the sea and the land; and do you not find a strange analogy to something in yourself? For as this appalling ocean surrounds the verdant land, so in the soul of man there lies one insular Tahiti, full of peace and joy, but encompassed by all the horrors of the half-known life. God keep thee! Push not off from that isle, thou canst never return!".

Moby Dick, Herman Melville,

ABSTRACT

The influence of particulate matter (PM) in the lower layers of the atmosphere is well known in the literature. In troposphere regions, particulate matter in storm clouds have influences in the growth of water droplets, reducing their average size as they act as condensation and freezing nuclei. Thus, the behavior of pristine and polluted atmospheres affects the development of storm clouds, intensifying the production of electrical discharges. Furthermore, the particulate matter absorbs and scatters the shortwave radiation emitted by the Sun, altering the radiative balance of the atmosphere and the surface. The backscattering of solar radiation due to particulate matter, causes a cooling effect of the lower layers of the troposphere, known as the Whitehouse Effect. Studies indicate that the increase of particulate matter in the atmosphere increases the lightning activity to a certain extent and as the concentration of particulate matter is further increased, the lightning activity decreases. As a result, a distribution of the number of electrical discharges in the shape of a “boomerang” is observed. These studies do not discuss a possible reason for this phenomenon. Thus, one of the hypotheses to explain this “boomerang” behavior is the Whitehouse Effect, in which the reduction of temperature in the lower layers of the troposphere caused by particulate matter, increases the atmospheric stability. In Brazil, the Metropolitan Region of São Paulo (MRSP) emits a significant amount of pollution, being a suitable place to study the influence of particulate matter and radiation on the lightning activity of storms. The present work shows possible evidence of the Whitehouse effect in the Boomerang effect. It was observed that the amount of shortwave radiation reaching the surface, decays due to the increase of aerosol concentration in the same way that the lightning activity also decays, indicating that the Whitehouse Effect can be the explanation.

Key Words: Boomerang Effect, Whitehouse Effect, Shortwave radiation, Metropolitan Region of São Paulo, Lightning activity, Particulate Matter, Aerosol.

A INFLUÊNCIA DA RADIAÇÃO SOLAR DE ONDAS CURTAS NA ATIVIDADE DE RAIOS NA REGIÃO METROPOLITANA DE SÃO PAULO: O EFEITO WHITEHOUSE

RESUMO

A influência do material particulado (MP) nas camadas inferiores da atmosfera é bem conhecida na literatura. Nas regiões da troposfera, o material particulado nas nuvens de tempestade influencia o crescimento das gotículas de água, reduzindo seu tamanho médio à medida que atuam como núcleos de condensação e congelamento. Assim, o comportamento de atmosferas pristinas e poluídas afeta o desenvolvimento de nuvens de tempestade, intensificando a produção de descargas elétricas. Além disso, o material particulado absorve e espalha a radiação de ondas curtas emitida pelo Sol, alterando o equilíbrio radiativo da atmosfera e da superfície. O retro-espalhamento da radiação solar devido ao material particulado causa um efeito de resfriamento das camadas inferiores da troposfera, conhecido como Efeito Whitehouse. Estudos indicam que o aumento de material particulado na atmosfera aumenta a atividade dos raios até certo ponto e, à medida que a concentração de material particulado aumenta, a atividade dos raios diminui. Como resultado, observa-se uma distribuição do número de descargas elétricas na forma de um "bumerangue". Esses estudos não discutem uma possível razão para esse fenômeno. Assim, uma das hipóteses para explicar esse comportamento em "bumerangue" é o Efeito Whitehouse, no qual a redução da temperatura nas camadas mais baixas da troposfera, causada pelo material particulado, aumenta a estabilidade atmosférica. No Brasil, a Região Metropolitana de São Paulo (RMSP) emite uma quantidade significativa de poluição, sendo um local adequado para estudar a influência do material particulado e da radiação na atividade de raios nas tempestades. O presente trabalho mostra possíveis evidências do efeito Whitehouse no efeito Boomerang. Foi observado que a quantidade de radiação de ondas curtas que atinge a superfície decai devido ao aumento da concentração de aerossol da mesma forma que a atividade de raios também decai, indicando que o efeito Whitehouse pode ser a explicação.

Palavras-chave: Efeito Bumerangue, Efeito Whitehouse, Radiação de Ondas Curtas, Região Metropolitana de São Paulo, Atividade atmosférica, Material Particulado, Aerossol.

FIGURES LIST

TABLES LIST

ACRONYMS

AOD	Aerosol Optical depth
ASHRAE	American Society of Heating, Refrigeration, and Air-Conditioning Engineers
CAPE	Convective Available Potential Energy)
CCL	Cloud Condensation Level
CCN	Cloud Condensation Nuclei
CETESB	Companhia Ambiental do Estado de São Paulo
CG	Cloud-to-Ground lightning
CGCT	Coordenação geral de Ciências da terra
DISSM	Divisão de satélites e sensores meteorológicos
GLM	Geostationary Lightning Mapper
IC	Intracloud lightning
INPE	National Institute of Space Research (From Portuguese: Instituto Nacional de Pesquisas Espaciais).
LF	Low Frequency
LFC	Level of Free Convection
LNB	Level of Neutral Buoyancy
MRSP	Metropolitan region of São Paulo
NOx	Nitrogen Oxides

PM10	Particulate Matter with a diameter < 1.0)
PM2.5	Particulate Matter with a diameter > 2.5 µm
UTC	Coordinated Universal Time
VHF	Very High Frequency
VLF	Very Low Frequency
VOCs	Volatile Organic Compounds.

INDEX

1- WORK MOTIVATION AND OBJECTIVES

This work aims to investigate the potential impact of shortwave radiation on lightning activity. Earlier research conducted in Amazon Rainforest done by Altaratz et al. (2010), found a relation between lightning activity and aerosols. Their findings indicated a boomerang effect in the lightning activity behavior in response due to aerosol. Farias et al. (2014) also found this same behavior over the Metropolitan Region of São Paulo (MRSP).

This boomerang effect shows an increase in lightning activity at lower levels of aerosol concentration, followed by a decrease at higher aerosol concentration. The underlying reasons for this behavior remain unexplained. Therefore, this work tries to propose the potential influence of the Whitehouse Effect on lightning activity. The Whitehouse effect is caused by the process of the incoming solar radiation reaching the top of the atmosphere and being then backscattered by the aerosol. This phenomenon may produce a cooling effect in the lower levels of the atmosphere and that can reduce the lightning activity. The research tried to find evidence of the radiation influence on lightning activity by considering that radiation and the aerosol relationship are significantly influenced by human activities in the Metropolitan Region of São Paulo (MRSP). The hypothesis of this research suggests that the radiation at surface decreases with an increase in PM10. As PM10 levels increase, there is a simultaneous increase in lightning activity. However, over particular PM10 concentration level, the lightning activity starts to decrease.

The following chapters will describe the main theoretical aspects of the work as well as the characteristics of the studied region, methodology and the instruments and the methodology adopted in this work.

2 - THEORETICAL FUNDAMENTALS

2.1- Introduction

This Chapter is based on works by Ahrens (2008); Cooray (2015); Williams (1995); Varejão (2006) and Houze Junior (2014) and briefly describes the cloud development, aerosols sources and formation, the lighting formation, and the interaction with radiation. These processes are physically interconnected and collectively contribute to the observed weather systems.

The formation of storm clouds has various stages: starting from the rise of the air parcel, the condensation of water within the clouds, their electrification and the effect of the aerosol on the formation of water droplets that subsequently influence precipitation and the lightning occurrence. Solar radiation is an important driver for cloud formation and development. Clouds consist of water droplets and ice particles suspended in the atmosphere and may include elements of dust, smoke, and industrial waste. Cumulonimbus, responsible for storm-formation clouds, have an anvil-like shape. Inside these clouds, the nucleation of water droplets directly depends on the radius of the condensation nuclei. In the saturation process, the presence of particulate matter from natural or anthropogenic sources suppresses cloud growth resulting in differences in polluted and pristine clouds (pristine clouds mean clean clouds, without pollutants). Additionally, this particulate matter tends to intensify storms and enhance the lightning activity. Cumulonimbus clouds generate lightning flashes due to the electrical charges inside their structures. The non-inductive model, explaining electricity within the cloud, outlines tripolar charge structure dependent on the particle's collisions, the medium temperature, and the presence of liquid water.

2.2 - Formation of storm clouds

The storm cloud formation starts with the transfer of solar radiation energy to the Earth's surface, increasing the temperature of air parcels near to the ground. As the temperature of the air parcels increases, their density becomes lower than that of the surrounding environment. This difference in density results in a

buoyant force, propelling the air parcels upward, transporting them to higher atmospheric levels. The temperature difference between air parcels and the surrounding environment is the primary factor leading to conditional or latent instability, which is the main convective storms driver, as shown in Figure 2.1.

Figure 2.1 - Cloud formation by air parcel due to two physical mechanisms: a) convection and b) orographic lifting.

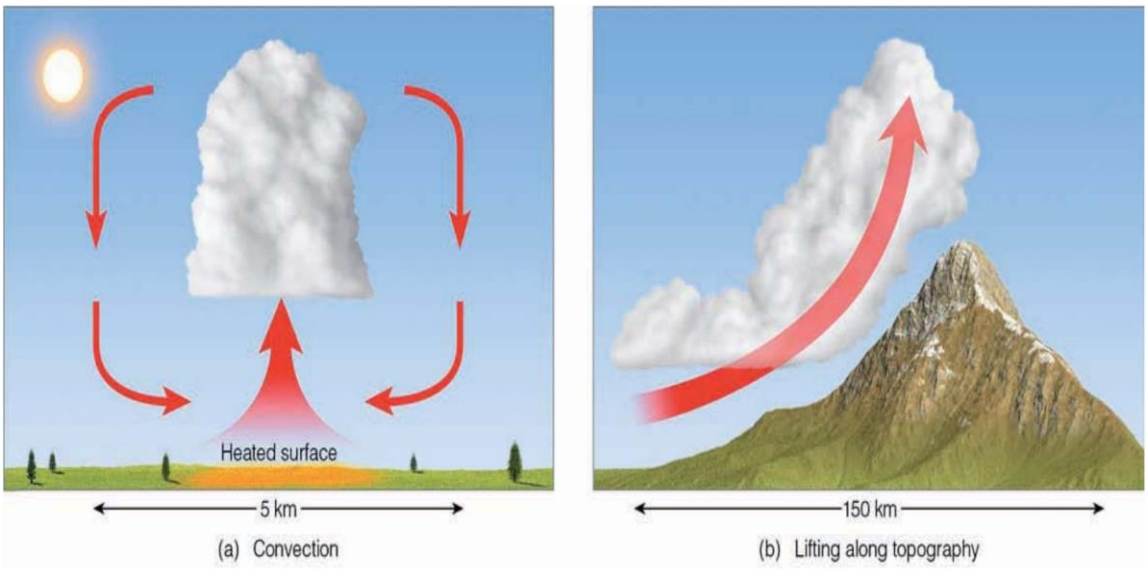

Source: Adapted from Ahrens (2008).

Air parcels are a discrete unit of mass isolated from the environment and their temperature changes as they ascend through the atmosphere.

The adiabatic processes in the atmosphere occur when there is no heat exchange between the system and the environment, which makes it possible to consider two convective processes that occur in the atmosphere:

- Unsaturated adiabatic convection
- Saturated adiabatic convection.

Both are described in next topics.

2.2.1 - Non-Saturated adiabatic convection

The initial process of storm cloud formation is only possible in unstable environments; therefore, the gravitational potential energy and the internal

energy of the parcel is particularly important for it to rise through the atmosphere without changing phase. As the air parcel rises through the atmosphere at a height rate given by (dz), the thermal energy of the air parcel converts to potential energy resulting in a decrease in the parcel's temperature.

All the equations which follow in Sections 2.2.1 and 2.2.2 are based on Williams (1995).

This process can be described by energy conservation, using Equation 2.1.

$$C_P \,.\, dT \; + \; g \,.\, dz \; = \; 0 \tag{2.1}$$

The thermal capacity of unsaturated air is C_P.

As the potential energy of the air parcel increases, there is a variation in its temperature, thus, the total variation in energy is zero, because there are no exchanges, and the rate is constant. Using Equation 2.1 to relate the temperature and the height in the atmosphere, the value of the unsaturated adiabatic gradient, Γ_d, is:

$$\frac{dT}{dz} = - \frac{g}{C_p} = \Gamma_d \; \approx \; 9,8\,^{\circ}C/km \tag{2.2}$$

Based on the value found in Equation (2.2 for each kilometer (km) that the air parcel rises in the non-saturated adiabatic convective processes, without changing its phase, its temperature decreases around 10 ºC. A fundamental quantity that influences non-saturated adiabatic convection is the potential temperature of the air parcel. Considering a pressure of p_o = 1000 mbar, the value of θ is obtained according to Equation (2.3):

$$\theta = T\left(\frac{p_o}{p}\right)^{\frac{R}{C_p}} \tag{2.3}$$

Equation (2.3) is known as Poisson's Equation, where R represents the unsaturated gas constant and R/c_p = 0,286, therefore:

$$\theta = T\left(\frac{p_o}{p}\right)^{0,286} \tag{2.4}$$

Thus, the air parcel will have a constant potential temperature when submitted to adiabatic transformations.

2.2.2 - Saturated adiabatic convection

In saturated adiabatic convection, the air parcel contains water vapor, therefore, the latent heat of condensation (L) must be included in the equation. The mathematical formulation of the adiabatic convection is given by Equation 2.5.

$$-L.\,dW_S = C_p.\,dT + g.\,dz \tag{2.5}$$

Where L = $2{,}5x10^6$ J/kg.

The dW_S rate describes the decrease in the amount of vapor in equilibrium in the air due to the increase in temperature caused by the release of heat during condensation. Therefore, rearranging the equation for the temperature rate in relation to the height rate (dT/dz) and considering Γ_s as a saturated adiabatic gradient as shown in Equation 2.6.

$$\frac{dT}{dz} = \frac{-\Gamma_d}{1 + \frac{L}{C_P}\frac{dW_s}{dT}} = -\Gamma_s \tag{2.6}$$

Due the fact of the rate dW_S/dT increases for the whole temperature's range considered. The conclusion is that: $\Gamma_s \leq \Gamma_d$.

2.2.3 - Distinction between stable and unstable atmospheres

This section is based on a description of the rise of air parcels in stable and unstable atmospheres based in Cooray (2015).

The Figure (2.2) below shows the behavior of air parcels in stable and unstable atmospheres. The left side of Figure (Figure 2.2.a) depicts a stable atmosphere, and the right side depicts an unstable atmosphere, (Figure 2.2.b).

Figure 2.2 - Differences in the rise of the air parcel in stable and unstable atmospheres.

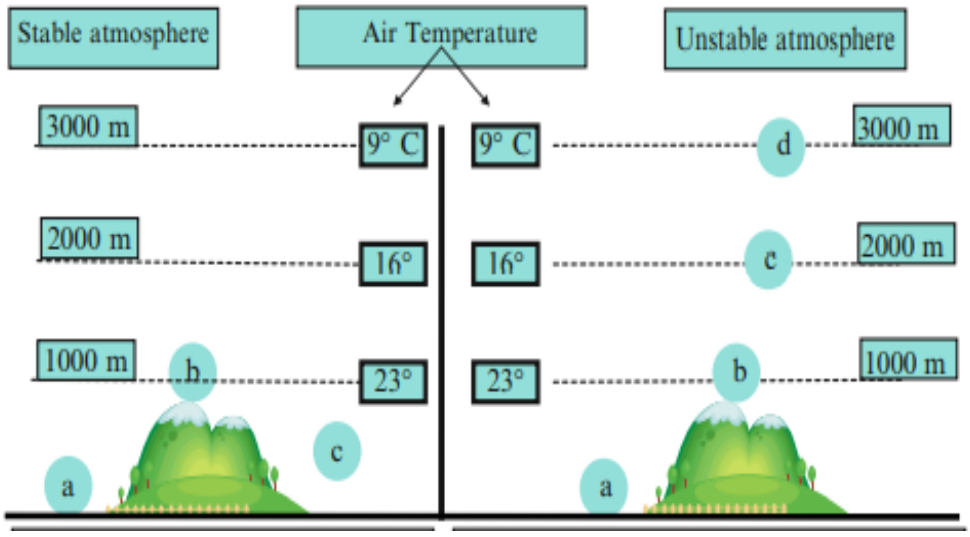

Source: Adapted from Cooray (2015).

According to Cooray (2015), the heat released by the condensation of the moisture present in the air parcel warms the air parcel. Thus, every 1000 m, the temperature of the air parcel drops by around 5.5°C. In stable atmospheres (Figure 2.2.a), the atmospheric temperature does not decrease very quickly, this

way, the temperature of the air parcel is lower than the surrounding environment, this leads to the interruption of the air parcel's rise throughout the atmosphere. On the other hand, when the temperature of the surrounding environment decreases faster, the air parcel will continue to rise as its temperature becomes higher than the surrounding environment. This phenomenon occurs in regions with an unstable atmosphere. So, the behavior of the air parcel is different in unstable and stable atmospheres.

Based on the description of Cooray (2015), considering the air parcel on (Figure. 2.2.a), describing a stable atmosphere.

A. At point (a) the air parcel rises along the mountain due to heating from the Sun.
B. At point (b), the air parcel cools at a certain height, resulting in a lower temperature than the surrounding environment.
C. At point (c), the temperature of the air parcel stops rising because its temperature is lower than that of the surrounding environment, causing the descent of the air parcel.

The Figure 2.2.b, describes an unstable atmosphere and based on the description of Cooray (2015), as following:

A. At point (a), the air parcel rises due to heating from the Sun.
B. At point (b), at the top of the mountain (1000 m), the temperature of the air parcel decreases, but is still higher than the surrounding environment, allowing it to continue to rise.
C. At point (c), the parcel remains lighter than the surrounding environment as its temperature continues to decrease, although it is still higher than that of the surrounding environment.
D. Finally, at point (d) the temperature of the air parcel continues to decrease but its temperature remains higher than the surrounding environment, allowing it to keep rising.

Thus, it is important to highlight that the main factors for the formation of a storm cloud are air humidity, dynamic mechanisms (mechanical forcing) and an unstable atmosphere.

The following sections details these aspects of thermodynamics, storm dynamics and cloud microphysics.

2.2.4 - Potential energy available for convection and parcel theory

It is possible to graphically describe the trajectory of the air parcel, starting from the Earth's surface until the neutral support level, known as tropopause, the highest region of the troposphere. The difference in temperature between the air parcel and the environment in a region higher than the convection level creates an area in the graphic known as CAPE (Convective Available Potential Energy). The CAPES is the amount of energy for storm development.

These concepts about CAPE are based on works done by Williams (1995).

The Figure 2.3 shows the process of ascension of the air parcel until reaching the tropopause. This plot is called Skew-T diagram. The dark blue line represents the tropopause that delimits the troposphere from the stratosphere. The orange line represents the temperature profile of the atmosphere. This temperature decreases monotonically until the tropopause.

At point 4, the orange line intersects the saturated adiabatic curve (The purple line). This is the Level of Neutral Buoyancy (LNB), where the temperature of the rising air parcel equals to the temperature of the environment.

Figure 2.3 - Skew-T diagram describing the rise of the air parcel in the formation of storm clouds.

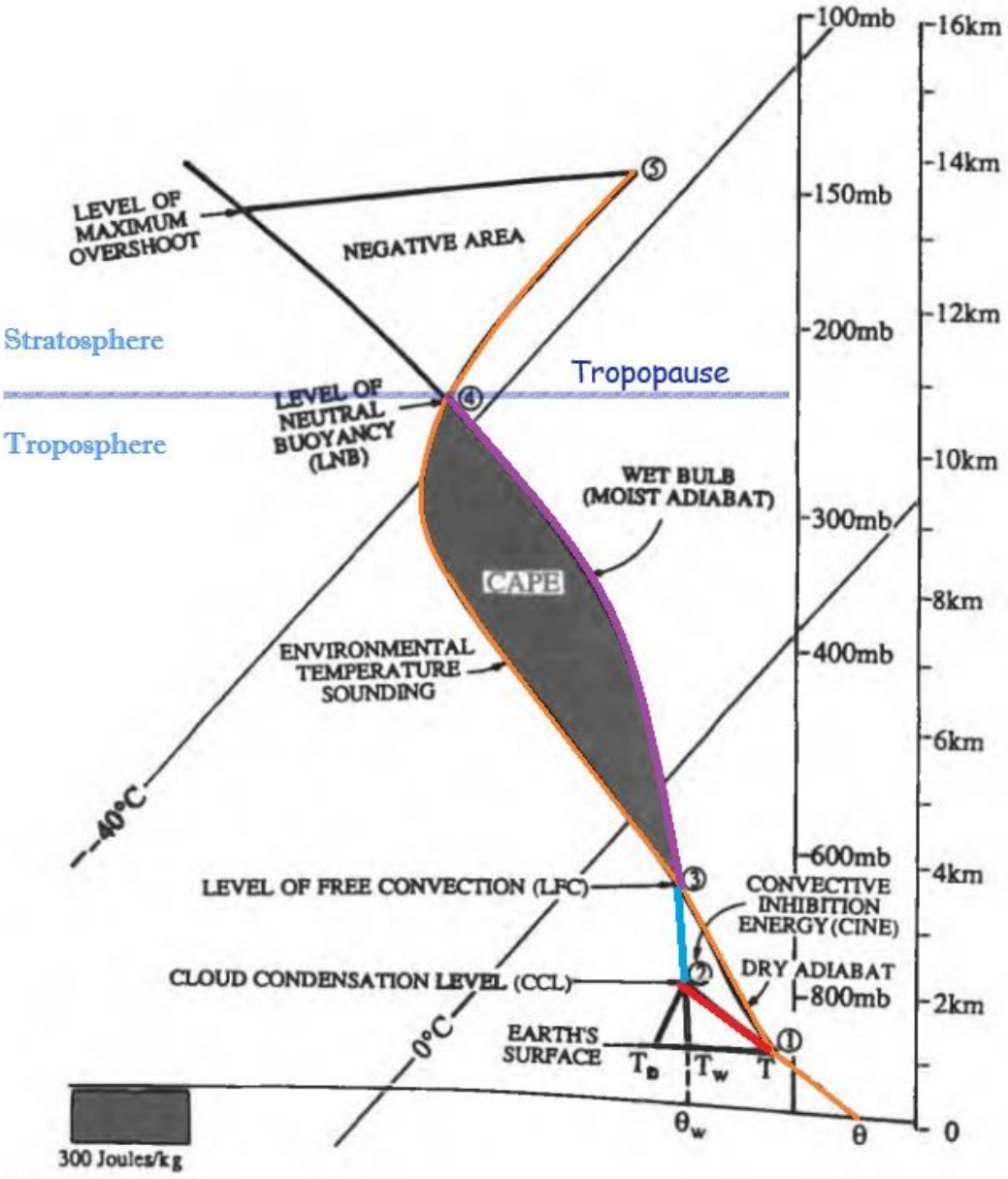

Source: Adapted from Williams (1995).

The path of the air parcel starts at Point 1, the red line represents mechanical forces that push air parcels up. This line follows the unsaturated adiabatic trajectory, which indicates the region where air parcel will rise adiabatically until it becomes saturated, reaching up the Point 2, the Cloud Condensation Level (CCL).

Along the unsaturated trajectory, the air parcel cools at a constant rate. When reaching Point 2, condensation begins and thus the cloud formation. This is the height of the base of the cloud. Beyond this point, the water vapor presents in the air parcel condenses, releasing heat. The trajectory of the air parcel represented by the light blue line, continues up to Point 3, known as the Level of Free Convection (LFC). This level represents the region where an air parcel becomes saturated when it rises adiabatically. At this point, the air parcel is at the same temperature of the environmental temperature's profile. If the air parcel continues to rise in the atmosphere, it will follow the purple line, the region where its temperature is always higher than the surroundings. The vertical ascending movements of the air parcel (called updraft) will cease when the air parcel reaches Point 4, the LNB. This region forms a plateau which is the top of the cloud.

The area between the purple and the orange line is known as CAPE, that is, the area delimited by the regions/points 3 and 4 (LFC and LNB). The Equation 2.7 describes the CAPE.

$$CAPE = \int_{LFC}^{LNB} \frac{T_{par} - T_M}{T_M} . \, g \, . \, dz \tag{2.7}$$

where T_{Par} is the temperature of the parcel and T_M is the temperature of the surrounding environment. Based on the CAPE, it is possible to compute the rising speed of the air parcel (updraft velocity), as described by Equation 2.8:

$$W_{(Z)} = \sqrt{2.(CAPE)_Z} \tag{2.8}$$

It is interesting to highlight that the speed $\boldsymbol{W_{(Z)}}$ at which the parcel rises into the atmosphere influences the size of the ice particles.

2.3 - Condensation of water vapor in clouds

As previously discussed, the presence of water vapor in the air parcel is fundamental for the formation of storm clouds and as the air parcel rises through the troposphere, the water vapor present in the air parcel condenses and forms water droplets. This section will describe how water droplets grow to form ice crystals and graupel (ice grains) and its role in cloud formation.

The water vapor is an important atmospheric constituent in temperature distribution, because affects the absorption and emission of heat in the atmosphere and transfers latent heat of evaporation, releasing heat when it condenses (HOUZE JUNIOR, 2014).

2.3.1 – Cloud Condensation Nuclei

This topic is based on works done by Hobbs (1993) and describes microphysics of the cloud.

Inside the cloud, water supersaturation processes occur influenced by the temperature in the cloud region and the radius of the existing cloud condensation nuclei (CCN). It is possible to find three regions of saturation:

1. Saturation - Standard temperature at which water changes phase.
2. Negative supersaturation - There is a phase change before reaching the saturation temperature.
3. Positive supersaturation - Does not change phase even at a temperature below the standard.

There are no flat surfaces in the atmosphere, therefore, it is not possible to consider an infinite radius to explain condensation. When considering the water vapor pressure on flat surfaces, there is an equilibrium of the vapor with the flat surface of the water given of e_s. The CCN surface has a curved shape and thus the saturation vapor pressure is higher than (e_s). Equation (2.9) describes the vapor pressure value that increases the flow of molecules towards the curved surface, called e_r. The vapor pressure e_r relates the molecular weight M, density ρ, surface tension σ and e_s, as:

$$e_r = e_s \exp\left(\frac{2M\alpha}{\rho RTr}\right) \tag{2.9}$$

In Equation 2.9 the molecular weight, density and surface tension refer to water data, respectively M= 18,02 g/mol, ρ = 1 g/cm^3, σ = 0,072 N/m, r represents the radius of the droplet, R = ideal gas constant, T = absolute temperature. The Equation 2.10 describes the saturation level of an atmospheric environment using the equilibrium of the vapor with the flat surface of the water (e_s).

$$S = 100\left(\frac{e}{e_s} - 1\right) \tag{2.10}$$

Homogeneous nucleation occurs in an environment where there is no presence of hygroscopic materials. Therefore, the need for high saturation makes homogeneous nucleation something that does not happen naturally in the atmosphere.

The heterogeneous nucleation occurs at much lower supersaturation levels compared to homogeneous nucleation and thus it is more natural to occur in the atmosphere. In this type of nucleation, water vapor more easily condenses over the aerosol's hygroscopic particles, which acts as CCN. The Heterogeneous nucleation occurs mostly in polluted atmospheres, so that the water vapor condenses over the CCN influenced by the presence of substances that do not volatilize, reducing the water vapor pressure. For solutions, this effect follows Raoult's law, where the value of e_s is reduced by a factor that depends on the solution concentration according to Equation 2.11:

$$e'_s = e_s N_w \tag{2.11}$$

where e'_s represents the vapor pressure of the solution (for a flat surface) and N_w represents the mole fraction of water in the solution.

The graph in Figure 2.4 shows the relation between the CCN radius and the saturation levels of different solutions. These are called the Köhler curves, and they define the relation between supersaturation of water, CCN radii and the concentration of the solution.

Figure 2.4 - Equilibrium supersaturation levels.

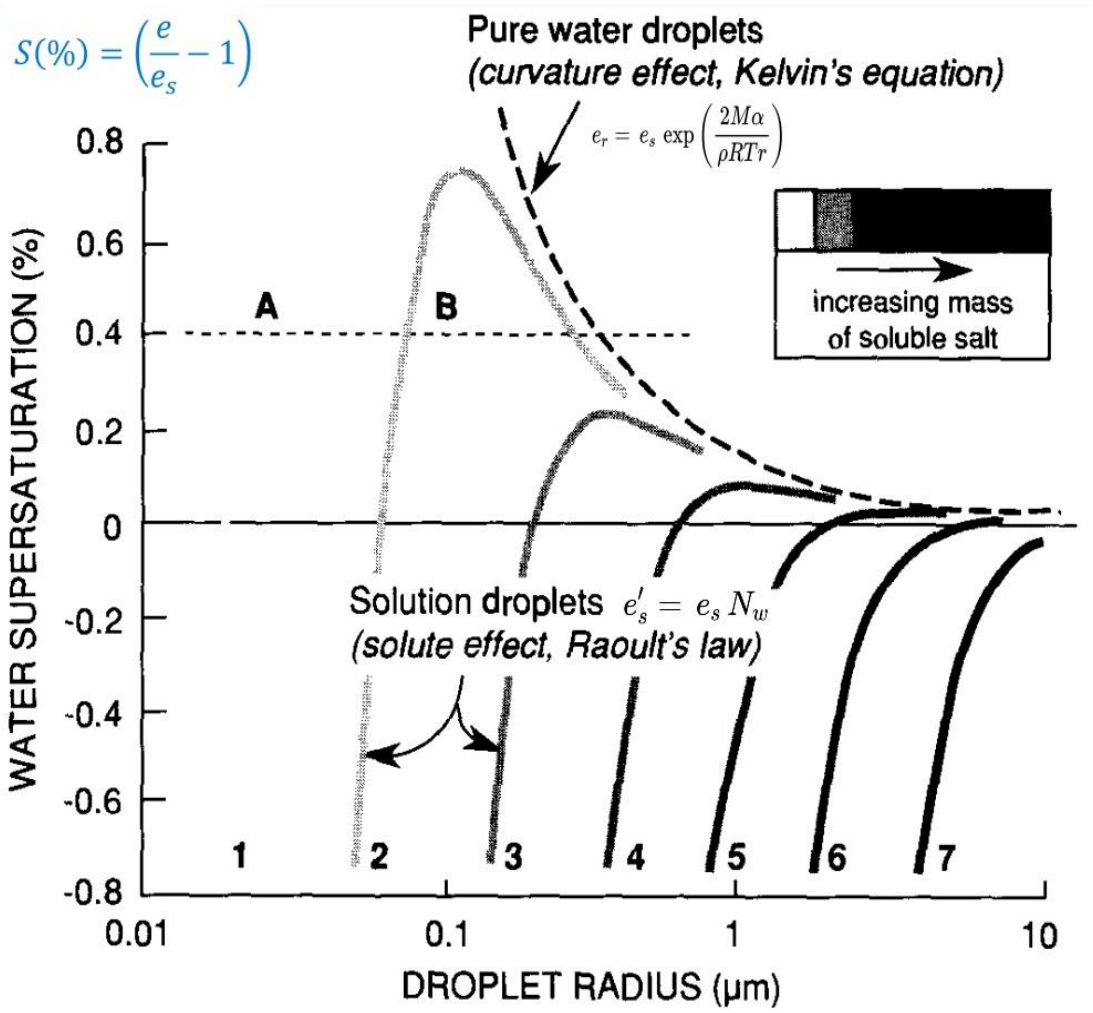

Source: Adapted from Hobbs (1993).

The dashed black curve describes the Kelvin equation. This curve shows that supersaturation decreases as the radius of the CCN increases. In the limit of infinite radius, the saturation level of the water is for a flat surface. As an example: for a CCN of 10 μm radius, droplets with will condense on a very lower supersaturation level, which is very close to the level for a flat surface. Considering a CCN of 1 μm radius, condensation will occur 20% above the flat

surface saturation level, which means, a supersaturation level of 0,2%. CCN smaller than 1 µm will not nucleate cloud droplets because they will require higher saturation level than the 10 μm radius CCN. For CCN of 0,1 μm radius, the supersaturation level will be greater than 100%, therefore, droplets will not condense easily in the atmosphere. Note that the supersaturation level for CCN activation reduces according to the amount of hygroscopic particles present with the cloud (according to the Raoult's Law). Furthermore, this effect is relevant for with small radii CCN, due to their low vapor pressure. Thus, the aerosols presence impacts directly on cloud microphysics reducing the size of water droplets by reducing the coalescence process. As a result, the amount of liquid water within a polluted cloud last longer compared to pristine clouds.

2.4 - Origin and influence of Aerosol in the atmosphere

This section described the influence of particulate matter on the formation of cloud particles (droplets and ice crystals); Also, the follow section describes the sources of aerosol emission, their characteristics and their influence on climate.

The information presented here on this section was based is based on Hobbs (1993); Seinfeld and Pandis (2006); Gelencsér (2005); Reist (1993).

The literature defines aerosol as particles suspended in the atmosphere emitted by diverse types of sources (natural or anthropogenic) with distinct distribution in the atmosphere. Natural emissions of aerosol come, for example, from volcanoes, ocean sea salt and vegetation. Anthropogenic emissions come from the cities, industrial processes, biomass burning, vehicles, emissions of nitrogen oxides (NOx) and sulfur dioxide (SO_2). Aerosol are classified in two categories: The primary and the secondary aerosol. The primary is emitted directly to the atmosphere by the source, while the secondary is formed in the atmosphere by chains of chemical reactions. There is a type of aerosol called organic aerosol that derives from the carbonaceous aerosol, i.e., particles that are mainly composed of carbon. The sources of organic aerosols also can be classified into two categories: The Primary Organic aerosol, which comes from direct emissions by vegetation, soil, ocean particles, bioaerosol and biomass burning. The

Secondary organic aerosol, which originate in the gas phase and is known as volatile organic compounds (VOCs).

2.4.1 - Diameter and deposition of particulate matter

This topic will describe specific characteristics of aerosols and is based on works from Reist (1993) and Johnson et al. (2011).

Particulate matter is distinguished based on its size, with fine particles with a diameter < 1,0 µm and coarse particles with a diameter > 2,5 µm. (PM10 and PM2,5, respectively). The size of these particles directly influences its behavior in the atmosphere and due to these differences in size, there are differences in their chemical structure, the sources that originate them, their interaction within the clouds and the method of deposition.

The most abundant fine particles, called fine mode, in the atmosphere are called nucleation particles. They are produced directly by combustion emissions and secondarily by nucleation, forming new particles. The size of these particles is around ~0,005 and 0,1 µm. There is also a second type of fine particles, called accumulation mode, which come from the coagulation of nucleus-type particles and the condensation of vapors on pre-existing particles. They grow then to larger sizes reaching up diameters of 0,1 to 2,5 µm.

The graph in Figure 2.5 shows the distribution of particulate matter by size and is divided into ultra-fine, accumulation and coarse modes. This difference in size distribution is due to the source that originate the particulate matter or how they are formed.

Figure 2.5 - Aerosol particle distribution by size.

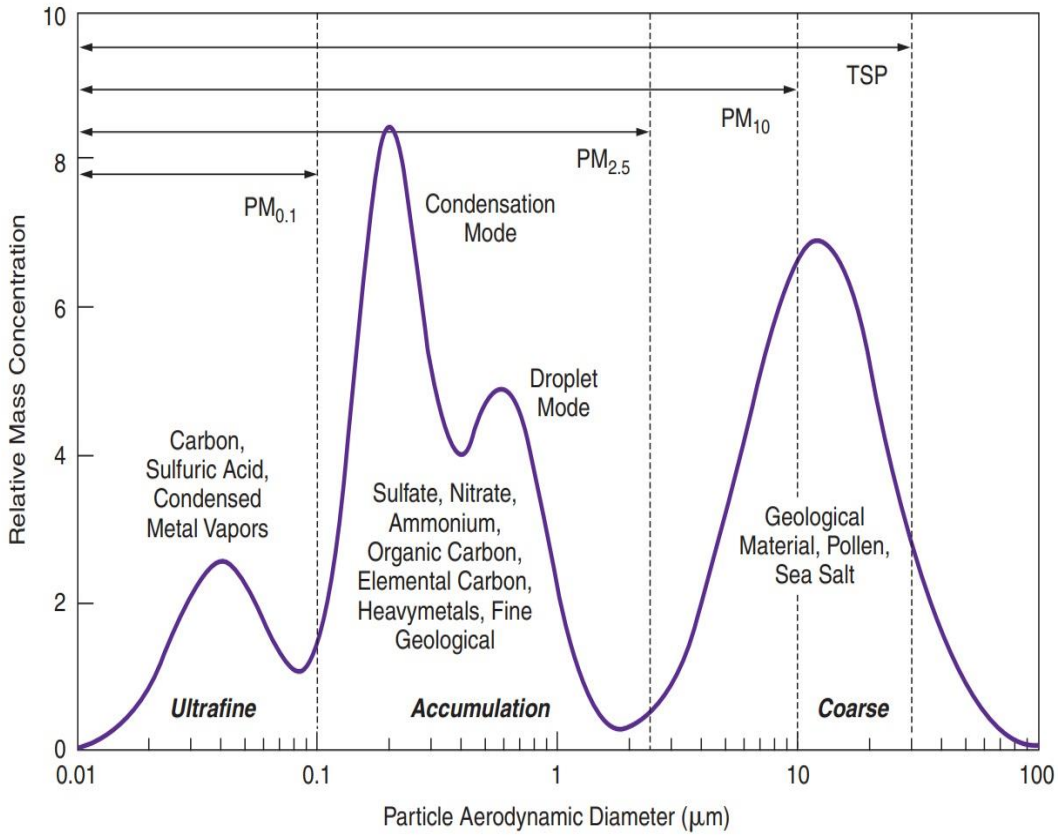

Source: Johnson et al. (2011).

Deposition methods are those responsible for removing the aerosols from the atmosphere, i.e., cleaning-like processes. They can be divided into dry and wet deposition. The first occurs through the sedimentation of particles towards the surface due to gravitational influence and diffusion. In wet deposition, aerosol particles are incorporated into raindrops and are removed by precipitation.

2.4.2 - Formation and behavior of pristine and polluted storm clouds

The aerosol has a huge influence in cloud formation. Processes are very different in haze and pristine atmospheres. This topic is based in works of Rosenfeld and Woodley (2001) and Rosenfeld et al. (2008).

Aerosol influences the development of storm clouds because it prevents the growth of water droplets, reducing their average size and distributing the liquid water among a large number of small droplets. (ROSENFELD; WOODLEY, 2001).

Since aerosol acts as condensation and freezing nuclei, the cloud life cycle is distinct in pristine (cleaner) and polluted atmospheres (with a strong presence of aerosol). The Figure 2.6 describes the evolution of pristine and polluted clouds.

Figure 2.6 - Evolution of cloud development in the pristine primitive atmosphere (above) and in the polluted atmosphere (below).

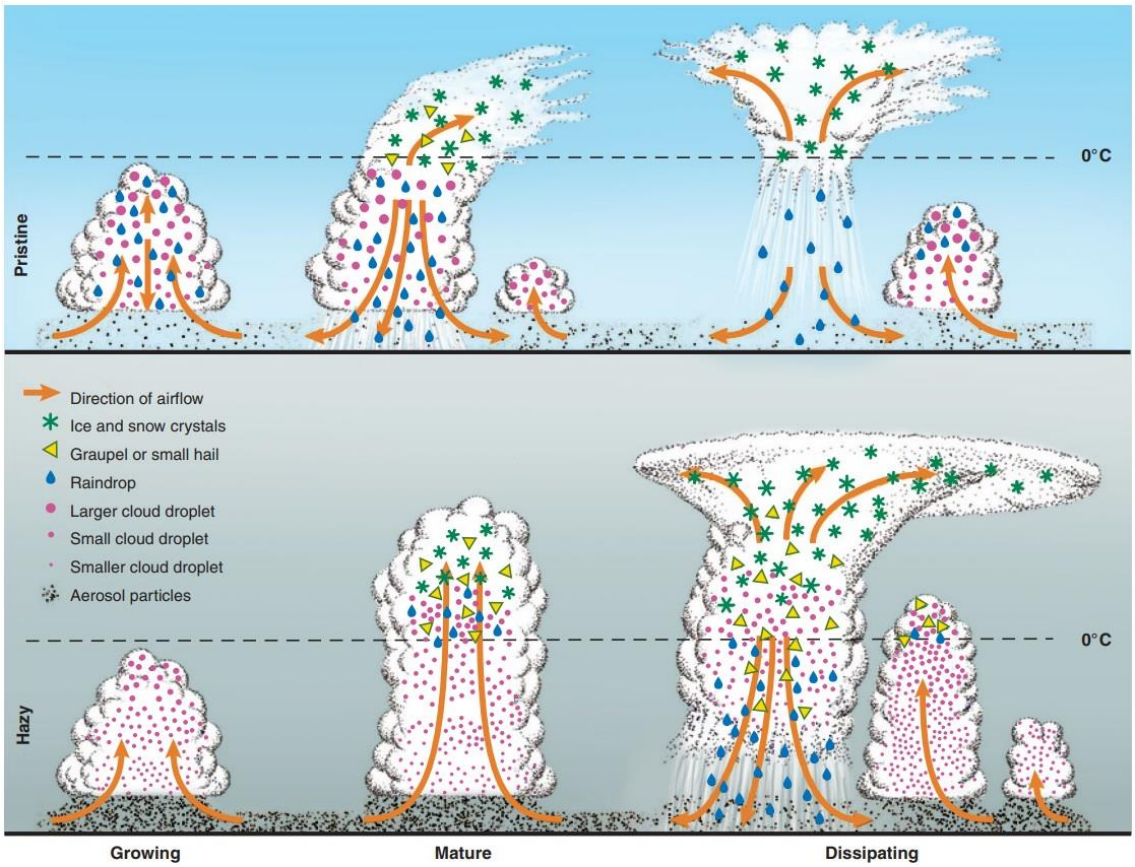

Source: Rosenfeld et al. (2008).

In the first stage, the water droplets in pristine clouds grow much larger than those in polluted atmospheres, which can quickly precipitate. On the other hand, in polluted clouds there is little competition between the droplets (due to the high concentration of CCN), which take longer to grow. Thus, they will not precipitate before reaching supercooling levels. At the second stage, when the clouds are mature, there is significant precipitation in the pristine cloud and the formation of some ice above the 0ºC isotherm. Meanwhile, in the polluted cloud there is almost no rain and thus most of the liquid water rises above the 0ºC isotherm. In the final stage, the pristine cloud has almost dissipated since most of water has already

precipitated. In the polluted cloud, the high amount of liquid water that reaches the higher altitudes releases latent heat, invigorating the convection. The stronger updrafts produce more ice, enhancing the storm. As a result, in polluted atmospheres, the clouds are invigorated by the presence of aerosols, producing intense precipitation and enhanced lightning activity. These effects will be discussed in the next sections.

2.4.3 - Formation of urban heat islands

The heat generated by cities produces the so-called heat islands, where the surface temperature is higher than its surroundings.

In urban areas, there is a massive emission of heat, as most of the surface is covered by asphalt and concrete, which store the incoming short-wave radiation as sensible heat releasing it back to atmosphere as long-wave radiation (STULL, 1988).

Also, the vehicle traffic and industry in the urban areas contributes to the heat island development because there is a temperature contrast between the urban and rural regions. Anthropogenic activities are the main cause of the formation of heat islands in cities, since they dramatically change the local environment by suppressing the vegetation and flattening and sealing the surface, in addition to pollution emissions. The removal of vegetation is an important factor in increasing temperatures. When comparing urban and rural environments, the lower temperatures are observed over green areas. Thus, microclimate of a city is distinct from regions of lower urbanization. The Figure 2.7 shows the pollutants carried by the breeze from the countryside to the city.

Figure 2.7 - Formation of heat islands in urban areas.

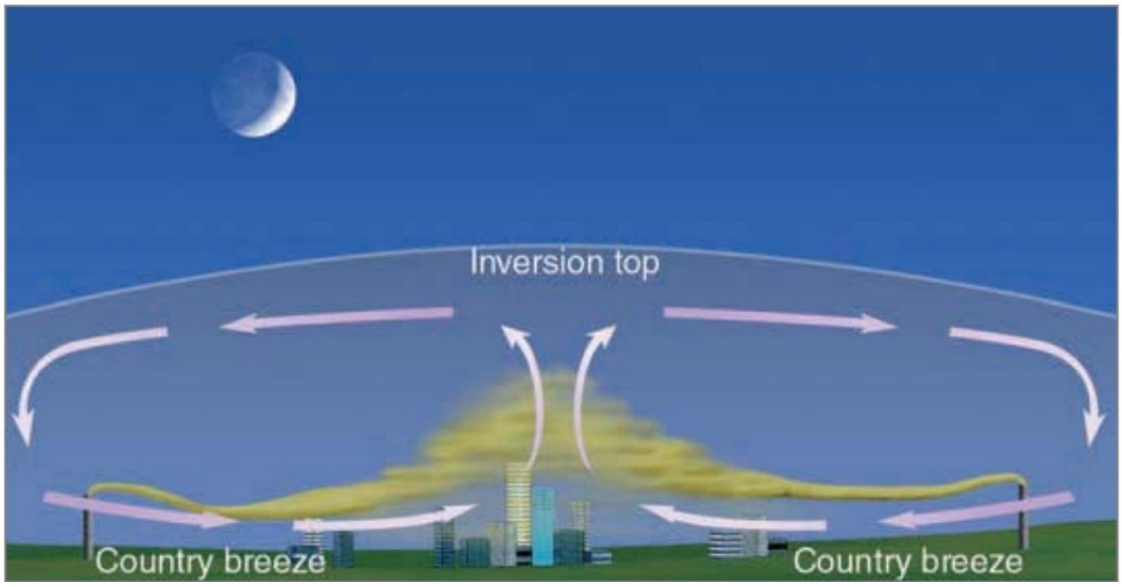

Source: Ahrens (2008).

2.4.4 - Aerosol in metropolitan region of São Paulo (MRSP)

Pollution in Metropolitan Region of São Paulo (MRSP) is very high due to the massive urban concentration. Particulate matter (PM10) is emitted by different sources. Vehicles and industries are the main sources. Particulate matter reaches high concentrations in winter, the season there are few rainy days to clean up the atmosphere.

The graph in Figure (2.8) below describes the relative emissions of both PM10 and other substances in 2022, according to the air quality report from CETESB, (2023), which shows that 31.2% of PM10 emissions in the MRSP originate from heavy vehicles.

Figure 2.8 - Relative emissions by type of source in 2022 – MRSP. The colors are: Light vehicles (Blue), industrial process (Orange), fuels base (yellow), heavy vehicles (red), resuspension (purple), total vehicles (beige), motorcycles (green), secondary aerosol (gray) and biomass combustion (pink).

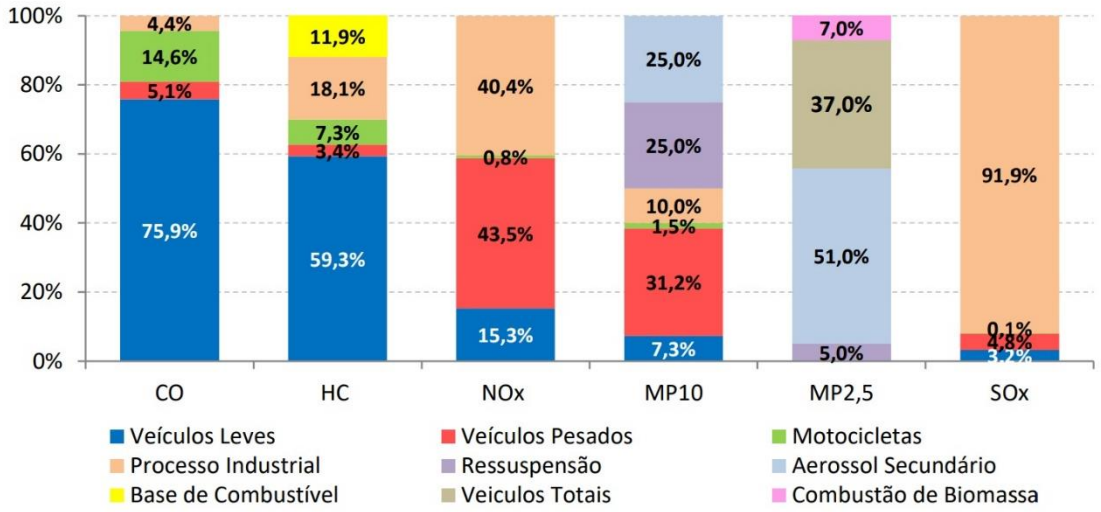

Source: CETESB (2023).

Based on data from 2022, the main sources of PM10 emissions in MRSP are the heavy vehicles, aerosol resuspension and secondary aerosols, which are produced by chemical reactions in the atmosphere from industrial and fuel emissions.

2.5 - Tripolar structure of storm clouds and lightning flashes

This topic discusses the tripolar structure of storm clouds based on studies from Saunders (1995) and Cooray (2015).

Several models have emerged to explain the electrical structure of clouds and currently the most accepted proposes that a storm cloud has positive and negative charges, distributed into three main centers. Electrification is produced by collisions between ice crystals and graupels in the presence of supercooled water. This model is called a collisional non-inductive model as in Figure 2.9. Non-inductive is because it assumes there is no external electric field contributing to the electrification of the cloud and Collisional because the process is based on

the collisions of ice particles within the cloud. Thus, charge separation occurs exclusively by charge transfer between graupels and ice crystal regardless of any local electric field (COORAY, 2015).

Figure 2.9 - Idealized tripolar structure of a storm cloud.

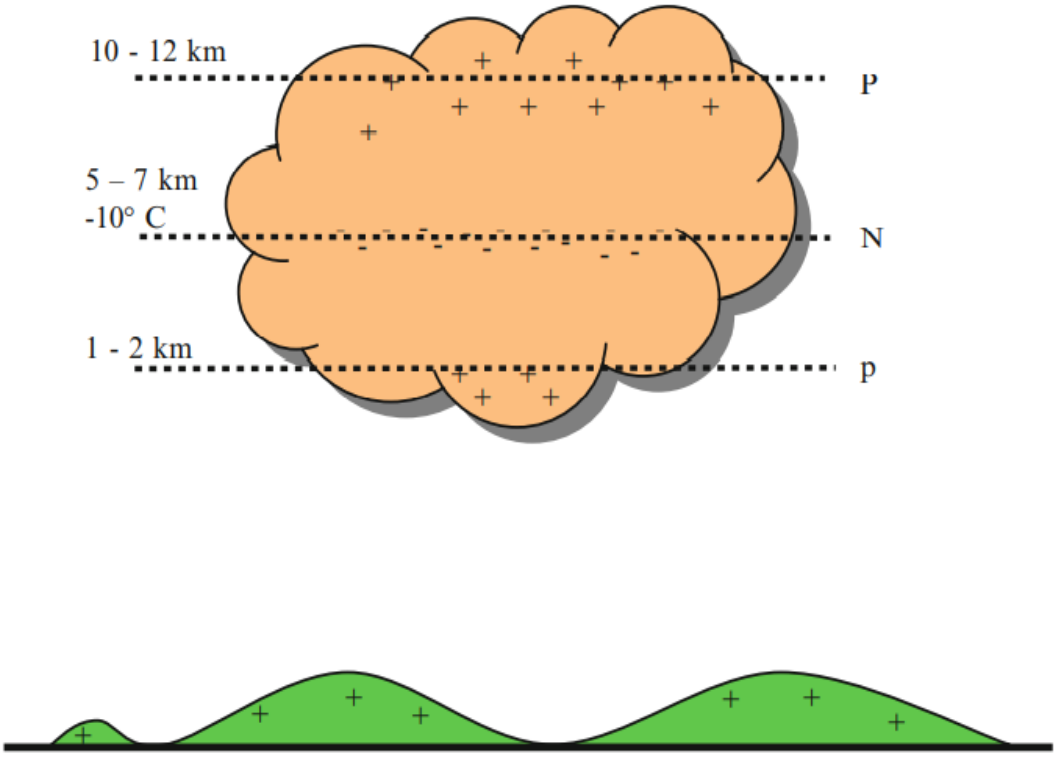

Source: Cooray (2015).

The two main charge centers are positive in the upper part of the cloud and negative in the middle of the cloud. A third, small positive charge center is in the base of the cloud. This configuration is mainly due to collisions between ice crystals (formed by vapor deposition) and graupels (formed by riming) in the presence of liquid water, as illustrated in Figure 2.10. The environment temperature is lower in the upper part of the cloud, so the collisions between the graupels and the ice crystals make them respectively negatively and positively charged. Since ice crystals are lighter than the graupels, they tend to stay in upper region of the cloud. Graupels, being larger and heavier, are kept in the mixed phase region of cloud (around the -10 ºC isotherm). In the lower region of the cloud, as temperature are higher, the graupels become positively charged while

ice crystals become negatively charged. Thus, the graupels tendo to remain closer to the base of the cloud, while ice crystals are kept higher in the mixed phase region of the cloud (-10 ºC isotherm). The -10 ºC is called the inversion temperature, which is the level where graupels and ice crystals invert the polarity of charge transfer after a collision.

Figure 2.10 – Charge transfer after collision of graupels and ice crystals showing the inversion temperature.

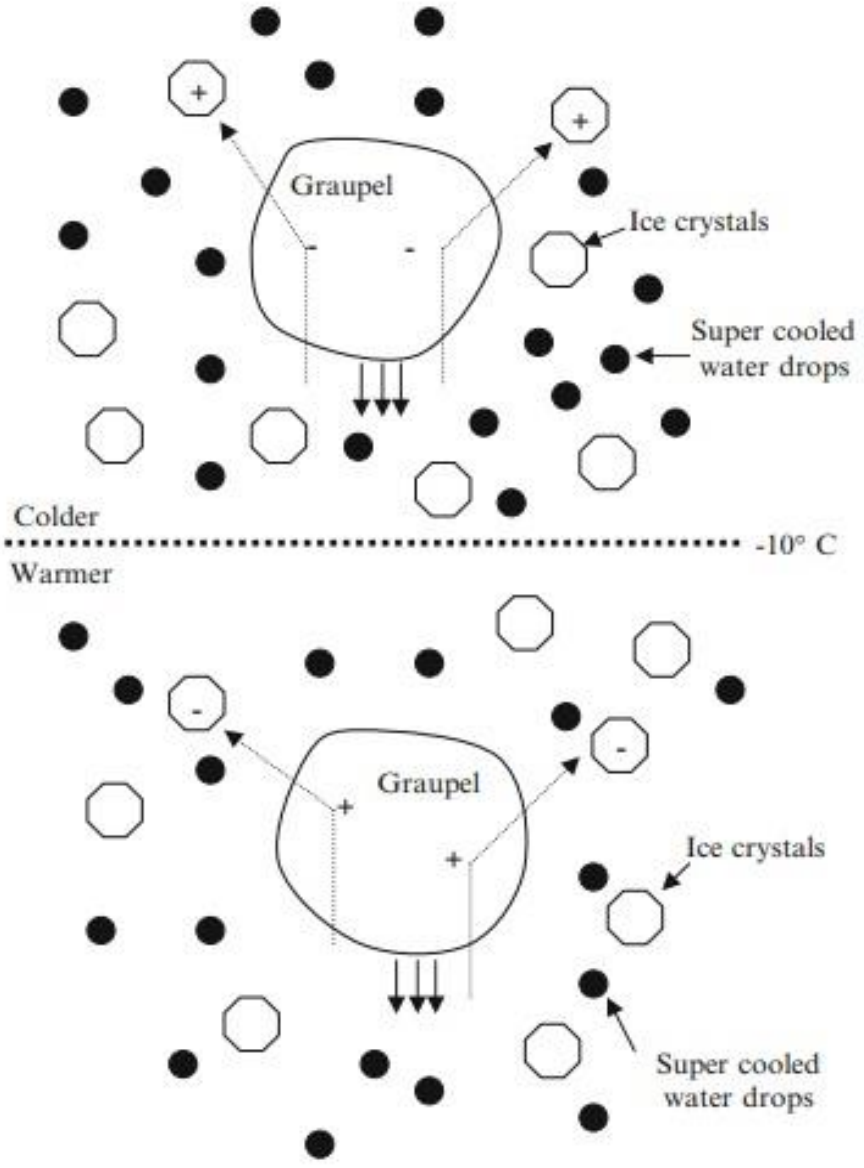

Source: Cooray (2015).

It is interesting to note that there is a fewer positive charge close to the base of

the cloud than in its upper region, where the positive charge center is much bigger. Since the temperature is higher in lower part of the cloud, graupels tends easily melt and precipitate compared to the upper part. Studies have shown that charge transfer between graupels and ice crystals depends on the temperature of the environment and the amount of available liquid water. This explains the differences in charging due to the collision of those particles. In the plot of Figure 2.11 it is possible to observe the charge transfer of graupel as a function of the inversion temperature.

Figure 2.11 - Charge transferred to a graupel by collision with ice crystals as a function of temperature. The inversion temperature corresponds to the point where graupel inverts its charge polarity.

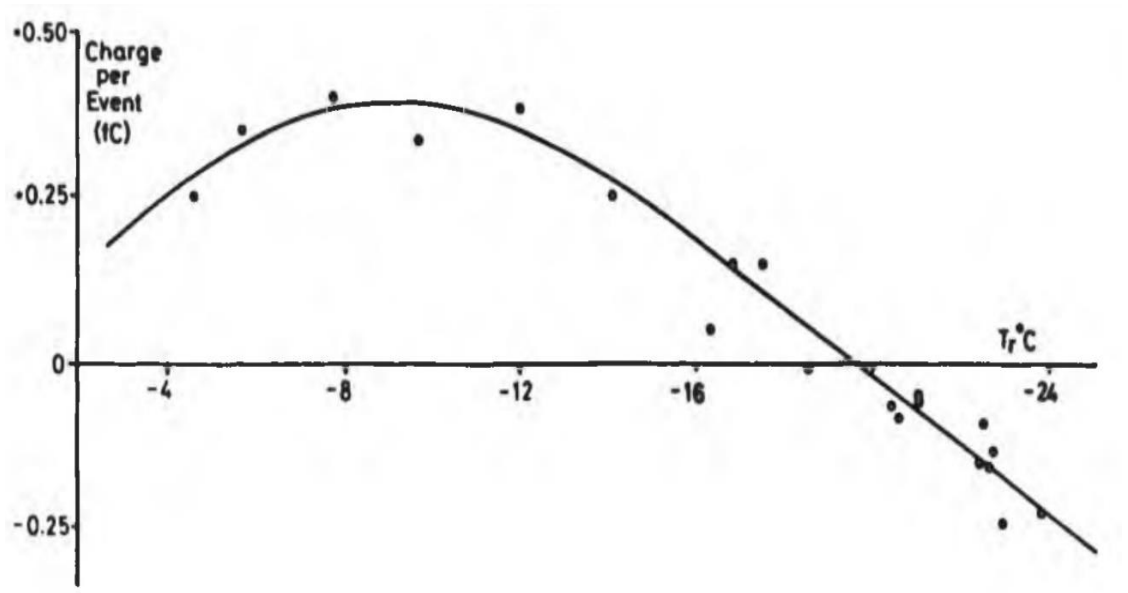

Source: Saunders (1995, p. 78).

In Figure 2.11, a greater quantity of positive charges is transferred to the graupels while temperatures are higher than -20°C. Below this temperature, negative charges are transferred to the graupel. Thus, -20°C is called the inversion temperature. The Figure 2.12 describes the charge signal transfer regimes as a function of effective liquid water content and environmental temperature.

Figure 2.12 - Sign of charge transferred to a graupel growing by riming through collisions with ice crystals as a function of the amount of effective liquid water and temperature.

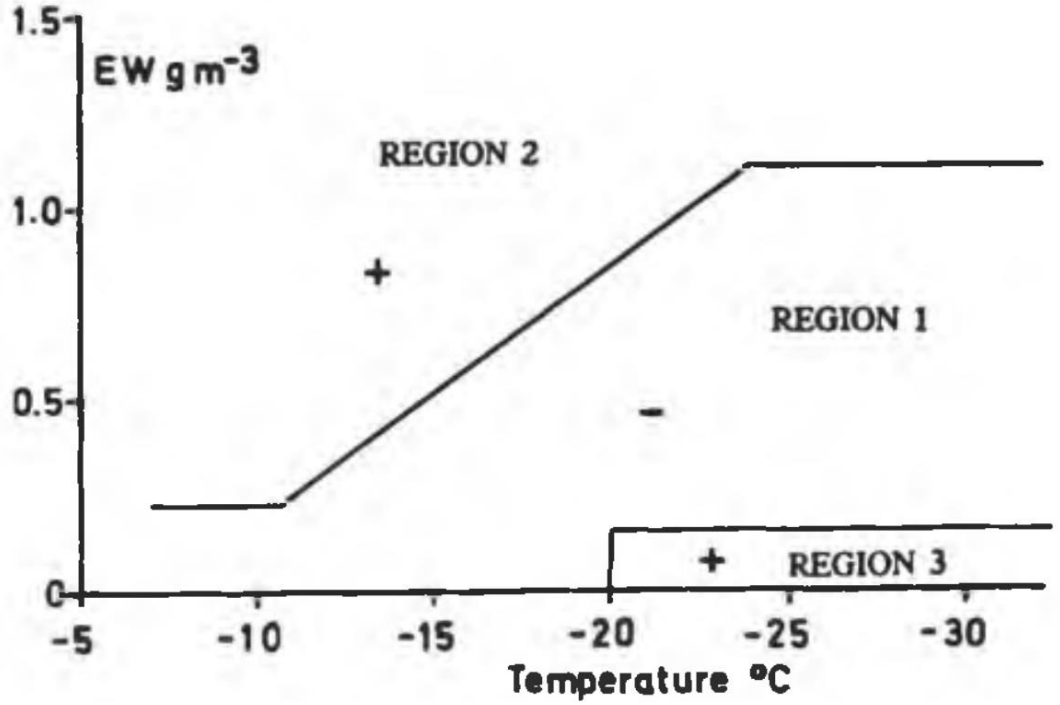

Source: Saunders (1995).

2.5.1 - The boomerang effect.

In recent work in the Amazon rainforest, Koren et al. (2008) used a theoretical model to analyze the connection between cloud coverage and their vertical development with the optical thickness of the aerosol (τ). The cloud coverage is expressed by the cloud fraction and based on the data obtained, the most polluted regions have the lowest fraction of clouds, describing a boomerang shape (Figure 2.13).

Increasing the optical thickness τ will inhibit the grow of shallower or small clouds, thus warming up the lower troposphere. On the other hand, clouds with high tops or with big area will cool down the lower troposphere (KOREN et al. 2008).

Figure 2.13 - The left plot describes the behavior of the relation of cloud properties and aerosol concentration (estimated by τ). The plot on the right shows cloud fraction versus τ.

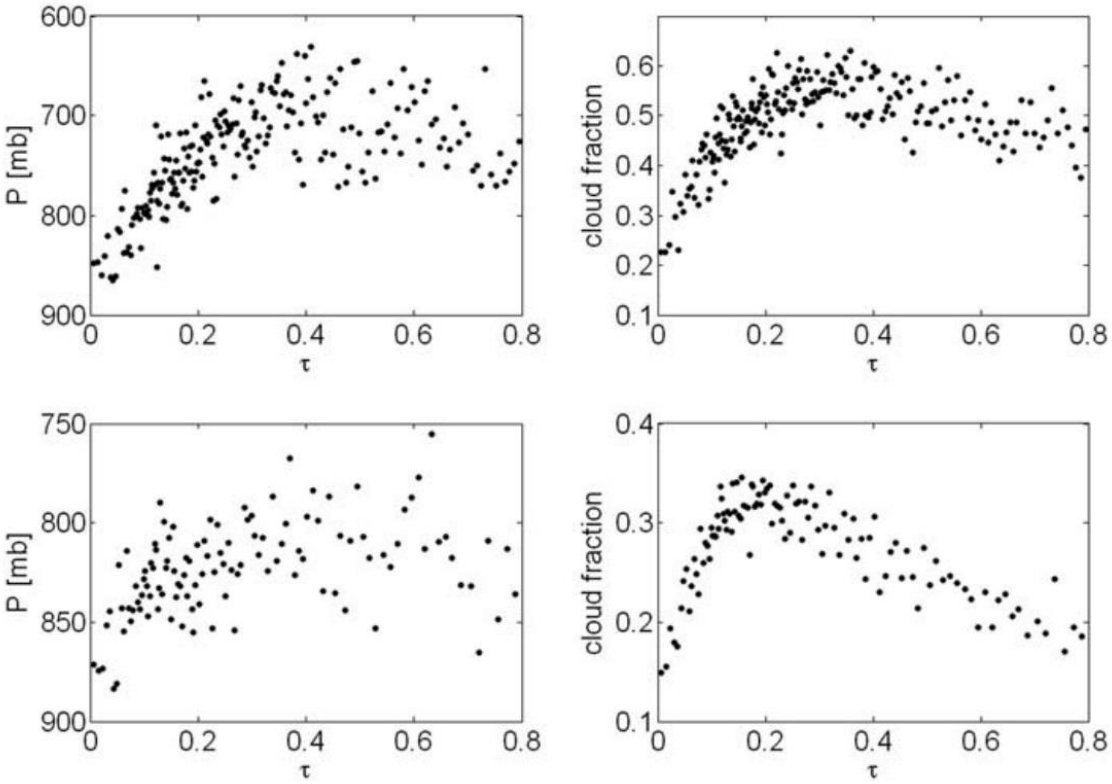

Source: Koren et al. (2008).

The boomerang-shape curves observed by Koren et al. (2008), were also observed by Altaratz et al. (2010), who analyzed the relationship of the lightning activity with the aerosol concentration.

Altaratz et al. (2010), examined the relationship between the structure of storm clouds and their electrical activity, as well as the effect of smoke in the Amazon region during four seasons (June-August 2006-2009)

The results (Figures 2.13) indicate that clouds with higher tops or big areas intense lightning activity. The correlation between the number of lightning and AOD shows the boomerang-shape behavior (Figure 2.14) and is similar to what Koren et al. (2008). The lightning activity increases proportionally to AOD until a particular level, beyond it the lightning activity decreases as the AOD continues increasing.

Figure 2.14 - Relationship between the lightning activity and AOD. The data is separated by years.

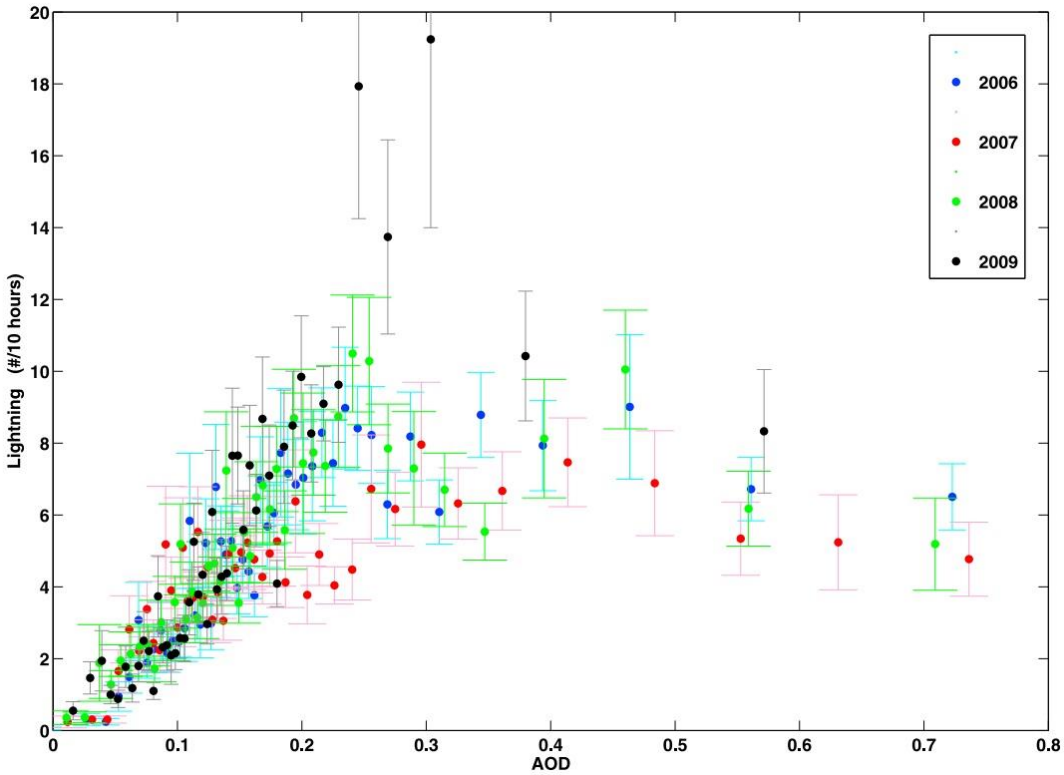

Source: Altaratz et al. (2010).

2.6 - Atmospheric radiation

This and next sections are based on works from Hinds (1999); Stewart and Mills (2021); Petty (2006), and they discuss the radiative balance, the albedo and the aerosol behavior when interacted with radiation.

The atmosphere can scatter and absorb the solar radiation and the environmental characteristics affect the transmitted radiation.

The main transference of energy in the atmosphere is electromagnetic radiation (LIOU, 2002).

The electromagnetic spectrum is classified into several ranges, from microwaves (lower frequencies) to x-rays (high energy particles) generated by nuclear reactions (PETTY, 2006).

Table 2.1- The electromagnetic spectrum observed in the Earth's atmosphere.

Region	Spectral range	Fraction of solar output	Remarks
X rays	$\lambda < 0.01\ \mu m$		Photoionizes all species; absorbed in upper atmosphere
Extreme UV	$0.01 < \lambda < 0.1\ \mu m$	3×10^{-6}	Photoionizes O_2 and N_2; absorbed above 90 km
Far UV	$0.1 < \lambda < 0.2\ \mu m$	0.01%	Photodissociates O_2; absorbed above 50 km
UV-C	$0.2 < \lambda < 0.28\ \mu m$	0.5%	Photodissociates O_2 and O_3; absorbed between 30 and 60 km
UV-B	$0.28 < \lambda < 0.32\ \mu m$	1.3%	Mostly absorbed by O_3 in stratosphere; responsible for sunburn
UV-A	$0.32 < \lambda < 0.4\ \mu m$	6.2%	Reaches surface
Visible	$0.4 < \lambda < 0.7\ \mu m$	39%	Atmosphere mostly transparent
Near IR	$0.7 < \lambda < 4\ \mu m$	52%	Partially absorbed, mainly by water vapor
Thermal IR	$4 < \lambda < 50\ \mu m$	0.9%	Absorbed and emitted by water vapor, carbon dioxide, ozone, and other trace gases
Far IR	$0.05 < \lambda < 1$ mm		Absorbed by water vapor
Microwave	$\lambda > 1$ mm		Clouds semi-transparent

Source: Petty (2006).

The solar radiation is called shortwave radiation and part of this radiation is scattered upwards by the clouds. Another part crosses the atmosphere reaching the surface. Shortwave radiation is represented by three bands of wavelengths: ultraviolet, the visible band and the near-infrared band. Solar radiation can cross

directly (S) or be scattered back by the clouds (diffuse radiation D). Direct and diffuse shortwave radiation is responsible for the total solar radiation (K↓).

$$K\downarrow = S + D \tag{2.12}$$

A fraction of this radiation that reach the surface are scattered back in the form of long-wave radiation, given by (L↑), as well is absorbed by the surface, given by (L↓). This process increases the temperature of the lower troposphere (greenhouse effect). The Figure 2.15 describes the approximated numbers of radiative balance of the Earth-Atmosphere system. It is possible to observe absorption and reflectance values in the atmosphere.

Figure 2.15 - Graphical representation of the radiative balance that occur in the atmosphere. The values approximated and is based on surface observations and satellite data.

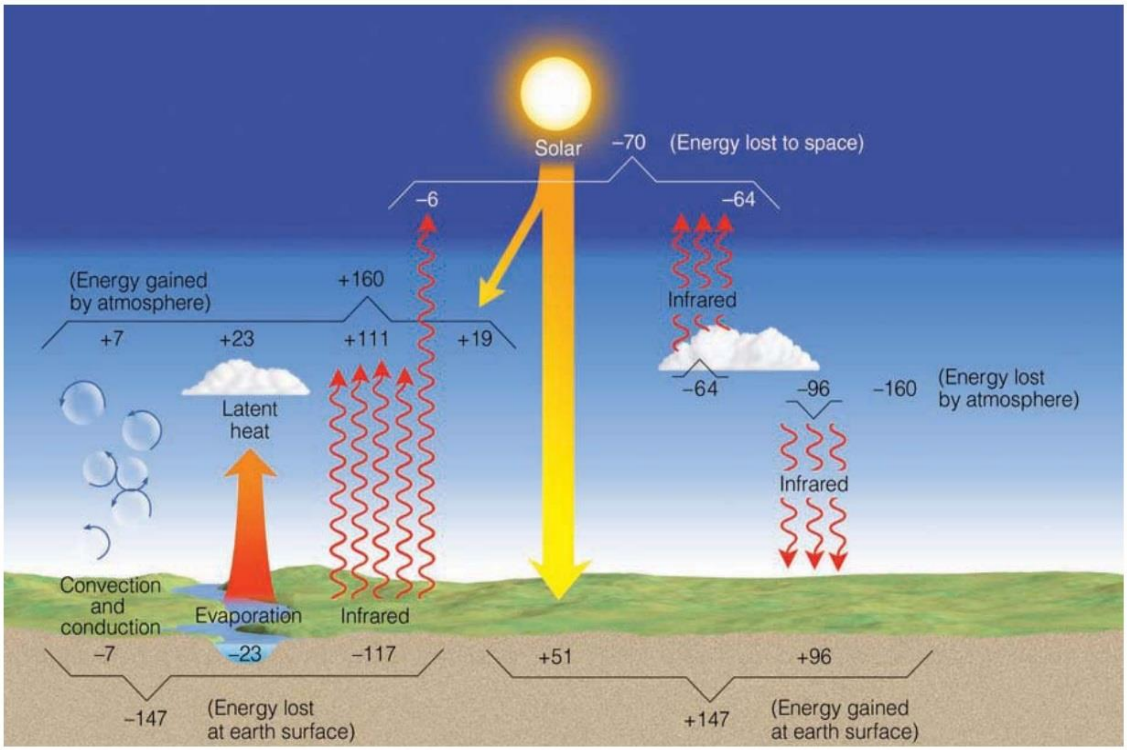

Source: Ahrens (2008).

Gases present in the atmosphere also absorb and emit solar radiation of different frequencies. The long-wave radiation scattered by the Earth's surface, for example, is absorbed by the greenhouse gases present in the atmosphere. This effect will be discussed in the next sections. In previous sections, the influence of

aerosol on cloud microphysics was described. However, the atmospheric aerosol also interacts with the solar radiation, warming up its layer (by absorbing radiation) and thus cooling down the underneath layers, reducing relative humidity and cloudiness also. It is interesting to note that when cloud coverage is low, larger areas of the aerosols are exposed to direct radiation of the Sun, heating the aerosol layer more effectively and thus reducing cloudiness even more.

2.6.1 - Influence of aerosols on the climate.

Since aerosols can absorb and scatter solar radiation in the atmosphere, they can affect the microclimate of a particular region. Furthermore, aerosols can also affect the planet's overall radiation balance, exerting a huge influence on the Earth's albedo (reflectivity).

According to Petty (2006), in terms of radiation scattering, an important characteristic is the particle size of the aerosols.

Briefly, albedo is the ratio between reflected and incident radiation, so its value is different according to the reflecting material. Therefore, it is possible to classify its value for different surfaces. Principal factors that can influence terrestrial albedo are:

- The type of land surface (composition and roughness),
- The frequency range of the incident radiation
- The direction in which the radiation reaches the surface.

Clouds are also efficient in absorbing radiation and thus is an important factor in keeping the planet warm. Furthermore, a dense layer of clouds can radiate back part of the absorbed radiation. Since atmospheric aerosol can scatter or absorb radiation, they it means that can cool down the lower atmosphere. As a result, it changes the temperature profile. These mechanisms modify the planet's radiation balance and can cool down its surface. Together they are called the Whitehouse Effect (HINDS, 1999).

2.6.2 - The greenhouse effect

In the greenhouse effect, the solar incoming radiation (shortwave radiation) reaches the earth’s surface and is scattered by the surface as longwave radiation.

According to Ahrens (2008), water vapor, CO2 and other greenhouse gases allow most of the shortwave solar radiation to reach the surface, but the long-wave radiation emitted by the surface is absorbed by these gases in different altitudes, causing a warming effect.

Thus, the greenhouse gases have a huge impact on climate change and, nowadays, there is a great concern about the point of no return, i.e., a threshold that if overpassed will make impossible to avoid global warming. In this case, there will be no effective solution for reducing the impact on the planet's temperature.

According to Stewart and Mills (2021), large and especially wealthy cities are the main emitters of anthropogenic CO2. These high of emissions are causing climate changes that generate more extreme weather events, such as heat waves and strong storms.

The Figure 2.16 describes the behavior of the longwave radiation in two different atmospheres: with and without greenhouse gases.

Figure 2.16 - Longwave radiation behavior in atmospheres without and with greenhouse gasses.

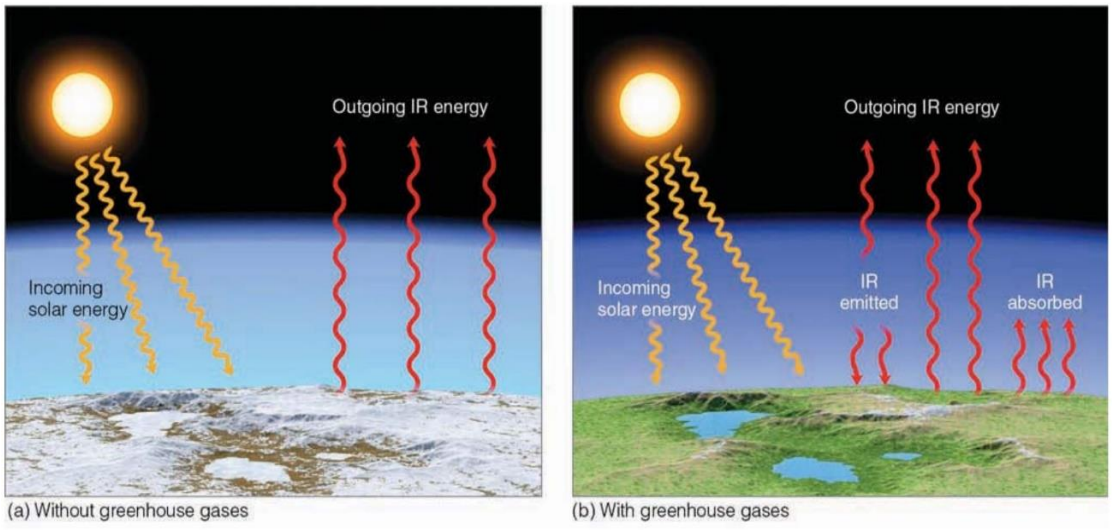

Source: Ahrens (2008).

2.6.3 - Whitehouse effect

The impacts of the greenhouse gases on the Earth's climate, are now well stablished since there are many published studies on this topic. In the previous section, there is a discussion on how the greenhouse gases cause a warming effect in the atmosphere. In this section, there is a discussion of an opposite phenomenon, called the Whitehouse effect. It occurs when solar radiation is backscattered by aerosols or clouds in the atmosphere.

Previous studies that discuss the interaction of aerosols with shortwave radiation do not mention anything about the concept of the Whitehouse effect, because there only few papers that specifically discuss the Whitehouse effect. The concept of the Whitehouse effect is presented by on Schwartz (1996), which is probably the first work to mention this effect.

The Whitehouse effect occurs when the incoming shortwave solar radiation is backscattered by atmospheric aerosol producing a cooling effect in the lower layers of the troposphere.

According to Schwartz (1996), there are essentially, two processes responsible for shortwave radiation reflection by Earth's atmosphere:

1. The first is called “direct effect”, caused by high concentrations of aerosol particles in cloudless atmospheres.
2. The second is the “indirect effect”, caused by an increase of aerosol concentrations that on their turn increases the small water droplet population in the clouds, thus increasing the radiation scattering.

The Figure 2.17 shows the radiation scattered by the clouds and the atmosphere:

Figure 2.17 – Average of solar radiation that is absorbed by the surface and the atmosphere.

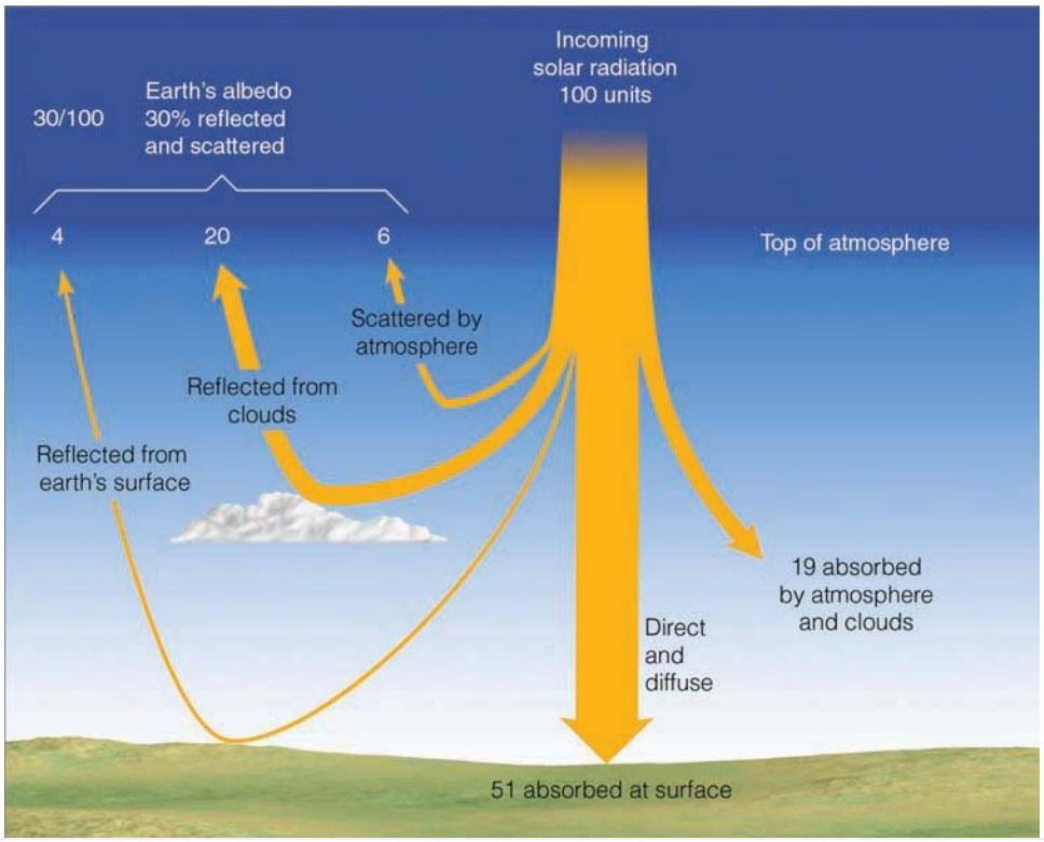

Source: Ahrens (2008).

The present work will focus on the direct effect, that means, situations where there are no clouds in the atmosphere and the shortwave radiation is backscattered by the anthropogenic aerosols.

According to Charlson et al. (1991), anthropogenic sulfate aerosols can backscatter the shortwave radiation reducing the radiance over the surface. These sulfate aerosols also act as cloud condensation Nuclei (CCN).

3 - METHODS AND MATERIALS

3.1 – General overview

This work aimed to find any correlation between the Whitehouse effect and the boomerang effect. The main idea is to find any evidence that the Whitehouse effect is suppressing lightning activity under hazy atmosphere conditions. Initially, the lightning activity and particulate matter (PM10) were both analyze to characterize the boomerang effect, as found by Koren et al. (2008) and Altaratz et al. (2010) in Amazon Rainforest and by Farias et al. (2012) in MRSP.

The lightning activity was also compared to the shortwave solar radiation that reached the surface. This approach intends to verify how the Whitehouse effect are connected to the boomerang effect. This analysis has not been done aforementioned authors.

As mentioned in Chapter 2, the shortwave solar radiation is backscattered and/or absorbed by the clouds and aerosols in the atmosphere. Thus, it might reduce the atmospheric instability since cools down the lower troposphere. As a net result, it is expected to reduce the lightning activity. Therefore, it is essential to find any connection between shortwave solar radiation reaching the ground, PM2.5, PM10 and lightning activity in order to find any relation of the boomerang and Whitehouse effect. As also described in Chapter 2, polluted atmospheres tend to produce more intense storms then pristine atmospheres, resulting in more intense lightning activity. Moreover, urban areas are responsible for the heat island effect, which warms up the local atmospheric boundary layer compared to their surroundings. In fact, Naccarato et al. (2003) showed that over densely urbanized regions, the lightning activity are modulated by changes in the local microclimate caused by the human activities. Since lightning is enhanced over urban environments, the MRSP was chosen to study a possible influence of the Whitehouse effect on the lightning activity.

Figure 3.1 – Urban area of MRSP.

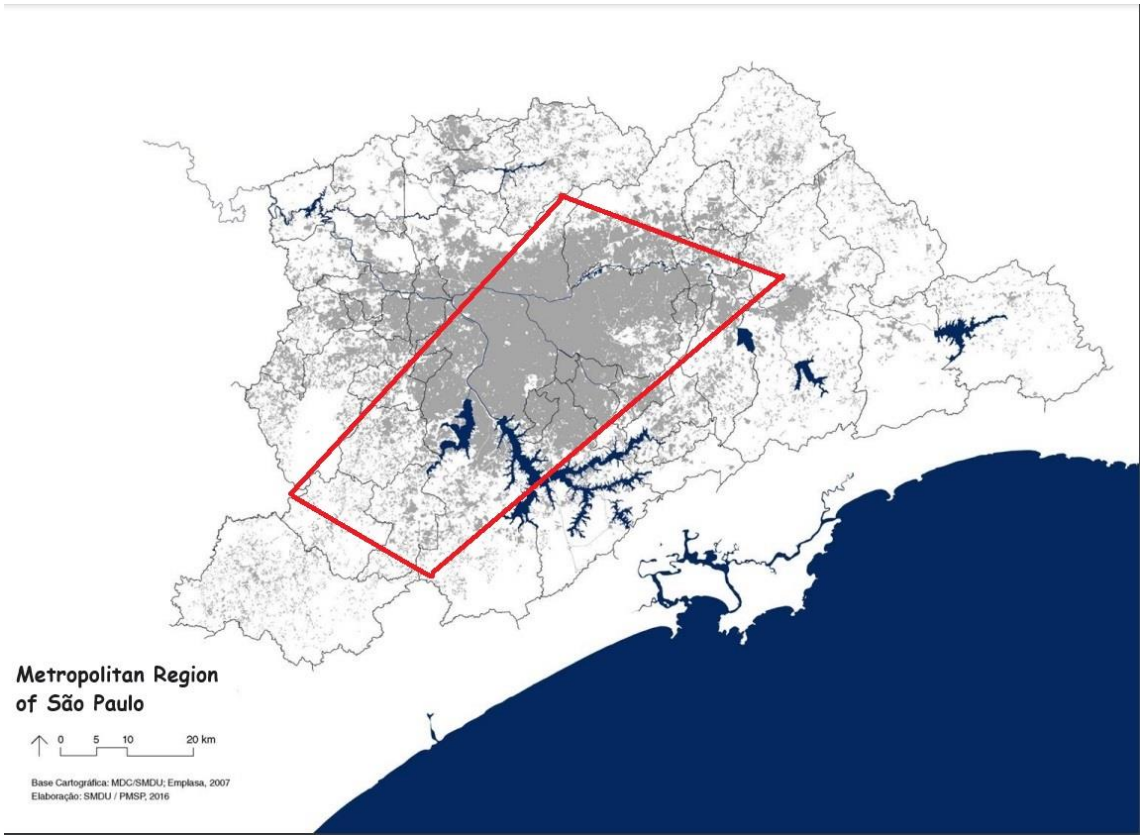

Source: Adapted from: Plano Metropolitano RMSP (2016).

The Metropolitan Region of São Paulo is composed of 39 municipalities and its total area is 7,946.96 km². The estimated population is 21,946,318 inhabitants according to the projections of IBGE (Brazilian Institute of Geography and Statistics) in 2022. The climate is very hot and humid during the summer and the winters are dry and cold.

3.2 – Lightning, particulate matter and the shortwave solar radiation data

Data used in this study were collected for a period of 5 years, from September 1st, 2019, to February 28th, 2023, over the Metropolitan Region of São Paulo (MRSP), a total of 1.277 days.

For a more detailed analysis, data was grouped into:

- Dry Season (April, June, July, August, September, October and November).
- Rainy Season (December, January, February and March).

Infrared GOES-16 images from DISSM/CGCT database were also used to select the best days for the study.

Since it is difficult to disentangle the solar radiation backscattered radiation by the aerosol and the clouds, it was selected 889 days (out of 1,277 days) with clear sky from 11 am UTC TO 5 pm UTC. The reason is to find days with clear sky before the possible lightning activity after 5 pm UTC. For the 889 days, the lightning data from GLM (Geostationary Lightning Mapper) onboard of GOES-16 satellite and from BrasilDAT lightning detection network were collected within the MRSP area (diagonal coordinates: -47.04 ºW, -23.84 ºS, and -46.1 ºW, -23.35 ºS). Only 142 days has lightning activity after 5pm UTC. Table 3.1 summarizes the numbers.

Table 3.1 – Criteria for selecting the best days for the study.

Total of days analyzed from 09/01/2019 to 02/28/2023.	**1,277**
Days with clear sky from 11:00h to 17:00h UTM.	**889**
Days with lightning activity detected after 17:00h UTM.	**142**

Source: By Author.

PM2.5 and PM10 data for the 142 days of clear sky before 17:00 UTM followed by lightning activity was measured by CETESB station of Parque D. Pedro II, located in a central region of the MRSP (coordinates: -23.550024 ºS; 46.628781 ºW). Theoretical (ASHRAE model) and observational (CETESB stations) data were also computed/collected in Parque D. Pedro II and were used to quantify the incoming shortwave solar radiation.

This work used three types of theoretical parameters:

- Extraterrestrial radiation, that which arrives at the top of the atmosphere.

- Theoretical ultraviolet (UV) radiation, which is calculated using the extraterrestrial radiation.
- Surface-level solar radiation for clear sky.

The observations provided by CETESB station are the UV and the global radiation.

The intensity of the incoming solar radiation varies as a function of the Sun's position related to Earth. Thus, the radiation data were collected from 10 am to 2 pm LT (1pm to 5pm UTC). The idea is to have the maximum energy reaching the ground, since the radiation flux is proportional to the cosine of the Sun's zenith angle related to Earth's surface. To quantify only the solar radiation that is backscattered by the aerosols, clarity indexes (Kt) were used. These indexes represent the atmospheric transmittances for different types of shortwave radiation. For this study, the clarity index of observed global shortwave radiation Ktobs(Global) was calculated for the same 142 days of lightning activity. The Ktobs(Global) is the ratio of observed global radiation and theoretical extraterrestrial radiation:

$$Ktobs(Global)=\frac{Radiation(obsGLOBAL)}{Radiation(Extraterrestrial)} \quad (3.1)$$

The possible effect of aerosols on solar radiation is studied by associating the PM10 and PM2.5 concentrations with Ktobs (Global) in attempt to find a reduction in the radiation index as the PM concentrations increases.

3.3 – Description of the infrared GOES-16 images

The GOES16 images data can be gathered from the DISSM / CGCT database available on internet: https://satelite.cptec.inpe.br/acervo/.

This work used the highlighted images from channel 13 (10.35 μm) on the Advanced Baseline Imager (ABI) sensor. The images are generated every 10 seconds and correspond to the radiance temperature of the top of the clouds. Figure 3.2 shows an example. The images were used to identify days with clear

sky since the clouds are highlighted by the processing algorithm allowing a relative accurate visual analysis.

Figure 3.2 – GOES16 image of ABI's channel 13 ((10.35 μm) over South America in 15/01/2023 at 1 pm UTC.

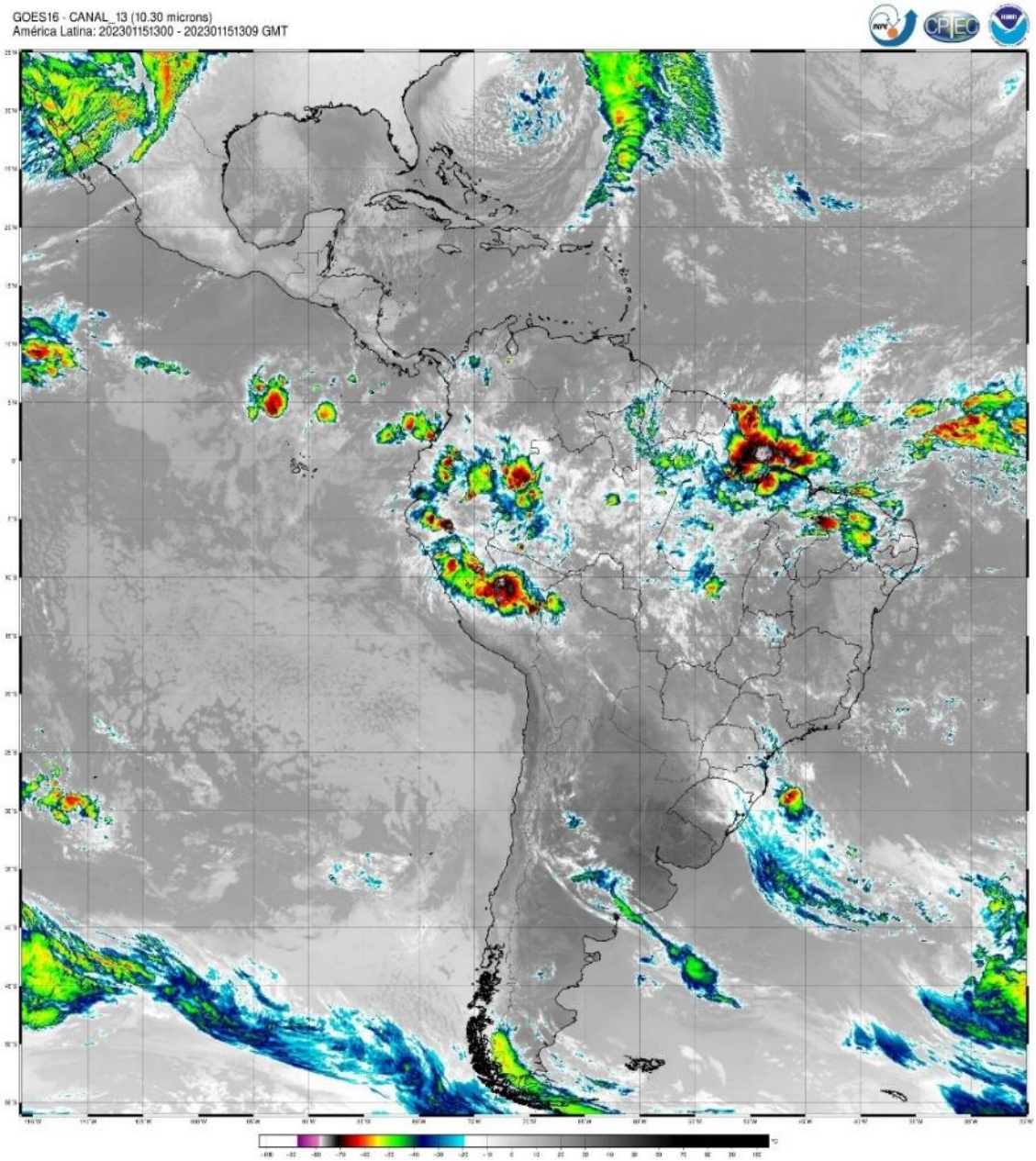

Source: DISSM / CGCT (2023).

3.4 - Description of GLM (Geostationary Lightning Mapper) dataset

The GLM is an optical near-infrared detector (777,4 nm) onboard of GOES-16 satellite that detect and geolocates optical pulses produced by lightning flashes over the entire America. The detection system produces data files every 20 seconds (GOODMAN et al., 2013).

The Table 3.2 shows a sample of lightning information provided by the GLM instrument.

Table 3.2 - GLM lightning samples.

Flash time offset of first event	Flash latitude	Flash longitude
2023-01-16 22:59:52	**-23,37471**	**-46,62923**
2023-01-16 22:59:23	**-23,37594**	**-46,61172**
2023-01-16 22:58:52	**-23,37923**	**-46,61455**
2023-01-16 22:58:34	**-23,37220**	**-46,60583**
2023-01-16 22:58:18	**-23,37217**	**-46,61924**
2023-01-16 22:58:03	**-23,37452**	**-46,60528**

Source: By Author.

3.5 – Description of the BrasilDAT lightning detection network.

The BrasilDAT lightning detection network was deployed by INPE during 2010 and 2011, starting operation in the end of 2011. It is composed by ground-based sensors installed over almost all Brazil that detect radiofrequency (VHF, LF and VLF) pulses emitted by the lightning. This system can discriminate cloud-to-ground (CG) to intracloud (IC) lightning and geolocate the CG events with less than 1 km error. The overall detection efficiency of BrasilDAT is more than 50% for IC events and 80% for CG events (NACCARATO; PERSONAL COMMUNICATION, 2023).

Figure 3.3 – Location of the BrasilDAT in 2022.

Source: Naccarato (2023).

Table 3.3 – BrasilDAT lightning data sample.

Date	Time	Nanoseg	Latitude	Longitude	Type of lightning
2020-09-30	17:31:57	368747308	-23.48686	-46.36934	1
2020-09-30	17:32:50	404769775	-23.49127	-46.36466	1
2020-09-30	17:35:16	728226323	-23.48217	-46.35655	1
2020-09-30	17:47:21	608088977	-23.54281	-46.43112	0
2020-09-30	17:47:40	280328178	-23.53926	-46.43619	1
2020-09-30	17:47:40	285167982	-23.51738	-46.44136	1
2020-09-30	17:47:40	431796763	-23.53259	-46.43405	0
2020-09-30	17:48:28	798364656	-23.52512	-46.43244	1
2020-09-30	17:50:22	475488582	-23.52969	-46.42278	1
2020-09-30	18:02:34	100250756	-23.50881	-46.35557	1
2020-09-30	18:03:34	355044621	-23.56305	-46.42485	1
2020-09-30	18:07:25	738271397	-23.58196	-46.39544	1

Source: By Author.

3.6 - Description of ASHRAE model

The ASHRAE (American Society of Heating, Refrigeration, and Air-Conditioning Engineers) model was used to provide theoretical solar radiation data assuming clear sky. This model allows predicting hourly radiation values over any region on Earth.

The description is based on Iqbal (1983) and Jamil and Khan (2014).

According to Iqbal (1983), the ASHRAE model is based in four main publications: Moon (1940), Threlkeld and Jordan (1958), Threlkeld (1963), and Stephenson (1967).

All the formulae in this topic were taken from Jamil and Khan (2014); Amarananwatana and Sorapipatana (2007) and ASHRAE (1985).

In summary, the model is based on three main constants: the apparent Solar radiation A (W/m²), the atmospheric extinction coefficient B (dimensionless) and the diffuse radiation factor C (dimensionless). These three constants are tabulated for each month of the year. Another important parameter of the model is the zenith angle, θ_Z , which is fundamental because the position of the Sun changes throughout the year. Thus, the amount of radiation that reaches the Earth's surface is different over the 365 days. The model provides estimates of hourly global radiation I which is related to the solar radiation hourly beam I_{bn} and the diffuse radiation I_D:

The hourly beam is given by.

$$I_{bn} = \text{A exp } (\frac{-B}{cos\ \theta_Z}) \tag{3.2}$$

$cos\ \theta_Z$ is the cosine of the zenith angle. The diffuse radiation is given by.

$$I_D = C.\ I_{bn} \tag{3.3}$$

In other words, the diffuse radiation is a constant sky diffusion factor multiplied by the solar the hourly beam. Based on I_{bn} and I_D: The daily global radiation is given by:

$$I = I_{bn} cos\ \theta_Z\ +\ I_D \tag{3.4}$$

The tree parameters that compose the cosine of the zenith angle equation are known as hour angle ω, the latitude of the station represented by φ and the solar declination δ. The cosine of the zenith angle thud is given by:

$$\cos\theta_z = \cos\delta\cos\varphi\cos\omega + \sin\delta\sin\varphi \tag{3.5}$$

The hour angle describes the angular distance between the local meridian and the celestial body (the Sun in this case) and each hour is equal to 15°. The hour angle is calculated using the solar time (ST).
The hour angle, given by ω:

$$\omega = 15°(12 - ST) \quad (3.6)$$

The solar time value of a region is calculated as:

$$ST = LT + ET/60 - 4/60(L_S - L_L) \quad (3.7)$$

L_S is the standard meridian for local time and L_L is the longitude in degrees.
The time equation (ET) is calculated as:

$$ET = 9{,}87sen2B - 7{,}53cosB - 1{,}50senB \quad (3.8)$$

3.7 - CETESB

CETESB operates several meteorological stations installed over the State of São Paulo, particularly over MRSP, providing weather, aerosol, and solar radiation data, such as: PM10 (particulate matter of 10 μm), PM2.5 (particulate matter of 2.5 μm) O_3 and SO_2 concentrations, wind speed and direction, precipitation, solar global and ultraviolet (UV) radiation. Data is collected hourly (in local time) and is available in a daily basis. Nowadays, CETESB has a network of automatic sensors to collect weather, aerosols and solar radiation which were used in this study.

Figure 3.4 – Pollutants hourly data and air quality indexes. The rating of air quality indexes varies from good (in green) to very bad (in purple).

Índice de Qualidade	0 - 40	41 - 80	81 - 120	121 - 200	> 200
Classificação	N1 - Boa	N2 - Moderada	N3 - Ruim	N4 - Muito Ruim	N5 - Péssima

Parque D.Pedro II - 01/01/2023

Hora	NO2 µg/m³		MP10 µg/m³			CO ppm			O3 µg/m³			MP2.5 µg/m³		
	Média Horária	Índice / Qualidade	Média horária	Média 24 h	Índice / Qualidade	Média horária	Média 8 h	Índice / Qualidade	Média horária	Média 8 h	Índice / Qualidade	Média horária	Média 24 h	Índice / Qualidade
01:00	27	5	89	21	17	0.8	0,5	2	30	43	17	69	16	25
02:00	--	--	93	25	20	--	0,5	2	--	40	16	59	18	28
03:00	20	4	58	26	21	0.5	0,6	3	22	35	14	36	19	30
04:00	26	5	70	29	23	0.5	0,6	3	17	30	12	32	20	31
05:00	29	6	33	30	24	0.4	0,6	3	13	25	10	14	21	33
06:00	30	6	28	30	24	0.5	0,6	3	11	20	8	12	21	33
07:00	27	5	21	31	25	0.5	0,6	3	16	19	8	16	22	35
08:00	25	5	29	32	25	0.5	0,5	2	32	20	8	12	22	35
09:00	18	4	1	30	24	0.3	0,5	2	47	22	9	13	22	35
10:00	16	3	14	30	24	0.3	0,4	2	65	28	11	15	22	35
11:00	10	2	69	32	25	0.2	0,4	2	83	35	14	11	22	35
12:00	8	2	27	32	25	0.2	0,4	2	89	44	18	3	22	35
13:00	5	1	0	32	25	0.2	0,3	1	95	55	22	1	22	35
14:00	10	2	0	32	25	0.2	0,3	1	84	64	25	3	22	35
15:00	12	3	51	32	25	0.4	0,3	1	111	76	30	27	22	35
16:00	9	2	66	33	26	0.3	0,3	1	113	86	34	21	22	35
17:00	11	2	73	35	28	0.3	0,3	1	115	94	37	43	23	36
18:00	7	2	24	35	28	0.3	0,3	1	96	98	39	29	24	38
19:00	11	2	6	35	28	0.2	0,3	1	85	99	39	20	24	38
20:00	15	3	8	35	28	0.3	0,3	1	71	96	38	32	25	39
21:00	13	3	36	36	29	0.2	0,3	1	59	92	37	24	24	38
22:00	12	2	18	37	29	0.2	0,3	1	50	88	35	8	24	38
23:00	9	2	39	38	30	0.2	0,2	1	49	80	32	10	23	36
24:00	8	2	30	37	29	0.2	0,2	1	53	72	29	8	22	35

Source: CETESB (2023).

Figure 3.5 – Weather and solar radiation hourly data from Parque D. Pedro II station.

Parque D. Pedro II - 01/01/2023

Hour	Wind speed m/s	Wind Direction Sector	Temperature °C	Relative humidity %	Atmospheric pressure mbar	UVA radiation W/m²	Global radiation W/m²
01:00	1.5	E	20.7	88	924	---	15
02:00	1.1	ESE	19.9	89	923	---	211
03:00	1.0	ESE	19.3	91	923	---	70
04:00	0.0	Calm wind	18.8	92	923	---	0
05:00	0.0	Calm wind	18.4	93	923	---	0
06:00	0.0	Calm wind	18.2	93	924	---	6
07:00	0.0	Calm wind	19.3	93	924	---	132
08:00	0.8	E	24.1	69	925	---	450
09:00	0.9	SE	25.6	60	925	---	525
10:00	1.1	SE	27.7	53	925	---	789
11:00	1.1	N	29.3	50	925	---	797
12:00	1.2	W	29.1	51	924	---	744
13:00	1.1	NW	29.5	49	923	---	517
14:00	1.0	SSW	28.4	53	923	---	250
15:00	1.6	S	25.4	70	923	---	398
16:00	1.4	S	27.1	58	922	---	650
17:00	1.4	S	25.3	72	922	---	180
18:00	1.5	SSE	24.8	72	922	---	94
19:00	1.2	S	23.4	77	923	---	32
20:00	1.1	SSE	22.5	80	923	---	0
21:00	1.1	S	21.5	83	923	---	0
22:00	1.0	SSW	21.4	83	924	---	0
23:00	1.3	ESE	21.4	81	924	---	0
24:00:00	1.1	ESE	21.1	81	924	---	0

Source: CETESB (2023).

4 - RESULTS

4.1 – The Boomerang effect

In the 142 days with lightning activity after 5pm UTC, different PM10 concentrations were observed each day with a maximum of 120 µg/m³. Moreover, since the PM10 concentration changes throughout the day, it was assumed the maximum value observed. Thus, the lightning activity were grouped into twelve PM10 bins (from 10 to 120 µg/m³ of the maximum PM10 concentration). Table 4.1 shows the average number of lightning events for all PM10 bins. Since GLM does not discriminate cloud-to-ground (CG) from intracloud (IC) events, data correspond to the total lightning (TL) activity. On the other hand, BrasilDAT network can distinguish between CG and IC events. Thus, both TL and CG events were analyzed. Appendix A shows a table with the 142 days of data. For each day, there are the amount of lightning events and the maximum PM10.

Table 4.1 - Bins of PM10 concentrations and averages of lightning for each PM10 bin.

PM10 bin (µg/m³)	Average number of TL events (GLM)	Averages number of TL events (BrasilDAT)	Average number of CG events (BrasilDAT)
10	0.27	0.1	0.07
20	13.47	10.77	1.92
30	26.01	29.83	13.66
40	53.9	63.68	19.28
50	27.71	59.03	16.8
60	29.84	38.54	12.86
70	26.03	38.51	11.56
80	16.79	68.14	8.49
90	15.63	4.9	2.88
100	2.4	2	1.13
110	2	0.9	0.08
120	27.67	7.03	0.87

Source: By Author.

Figure 4.1 shows the correlation of the number of lightning events detected by GLM and BrasilDAT and PM10 concentrations. BrasilDAT data is categorized into TL and CG events. The graphic plot was based on Table 4.1.

Figure 4.1 - Boomerang effect observed over the Metropolitan Region of São Paulo. The blue line corresponds to TL events detected by GLM; red line corresponds to TL events detected by BrasilDAT; and the yellow line corresponds to CG events detected by BrasilDAT.

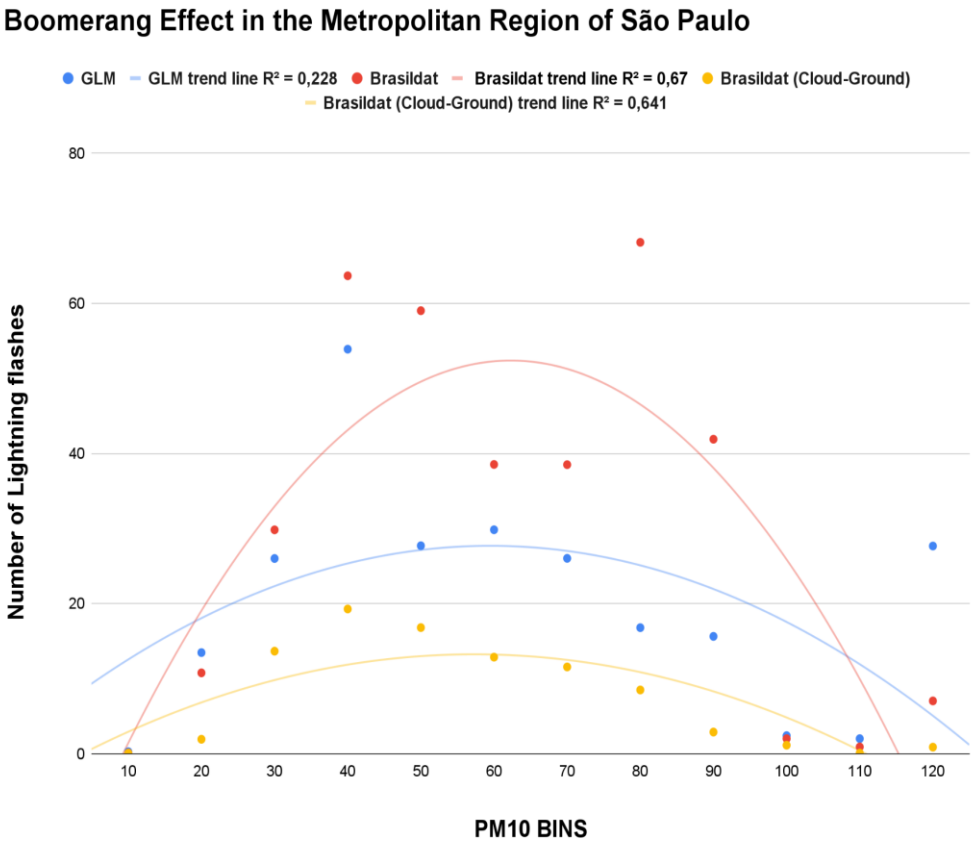

Source: By Author.

Figure 4.1 shows that the number of lightning events increases proportionally to PM10, until around 60 µg/m³. For higher PM10 concentrations, the lightning activity starts to decrease. This boomerang trend is more prominent for BrasilDAT TL data (red line) with R^2 = 0.67. The CG lightning data presented $R^2 = 0.64$ and GLM only $R^2 = 0.23$.

4.2 - Ktobs (Global) clarity index

Figures 4.2 and 4.3 describe the correlation of global clarity index Ktobs(Global) and PM10 concentrations for rainy and dry seasons, respectively. The plots are based on data from Table 4.2. Both figures show that the amount of solar global radiation reaching the Earth's surface decreases with the increase in PM10. However, for the rainy season the correlation is much higher ($R^2 = 0.73$) compared to the dry season ($R^2 = 0.14$).

Figure 4.2 - Behavior of Ktobs(Global) for the rainy season in terms of PM10 concentrations.

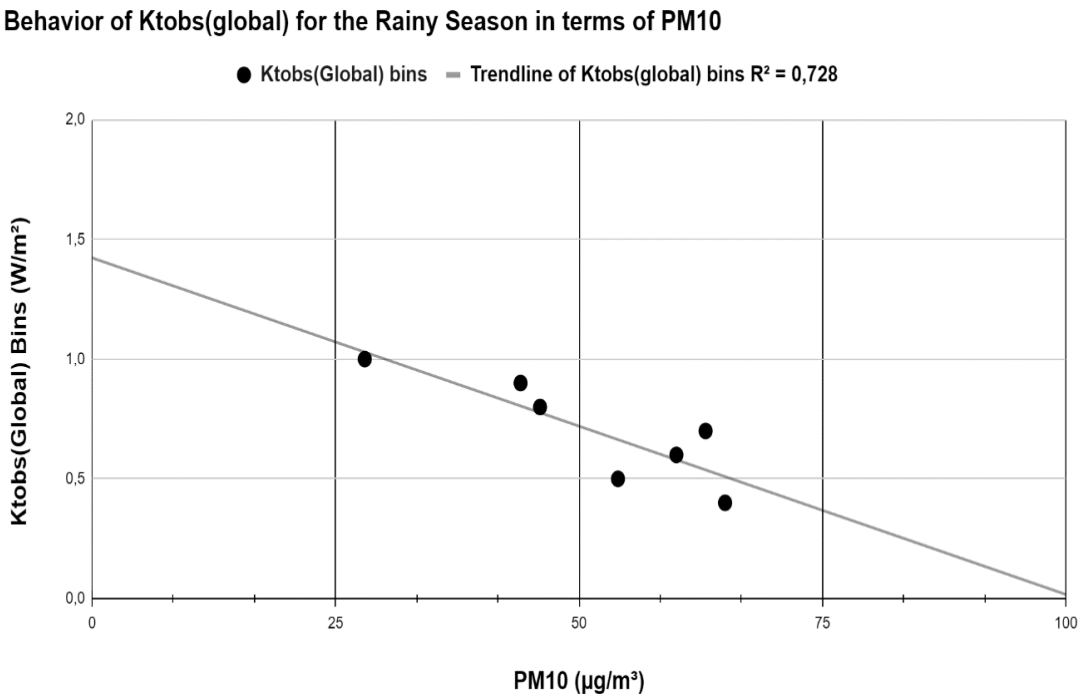

Source: By Author.

Figure 4.3 - Behavior of Ktobs(Global) for the Dry Season in terms of PM10.

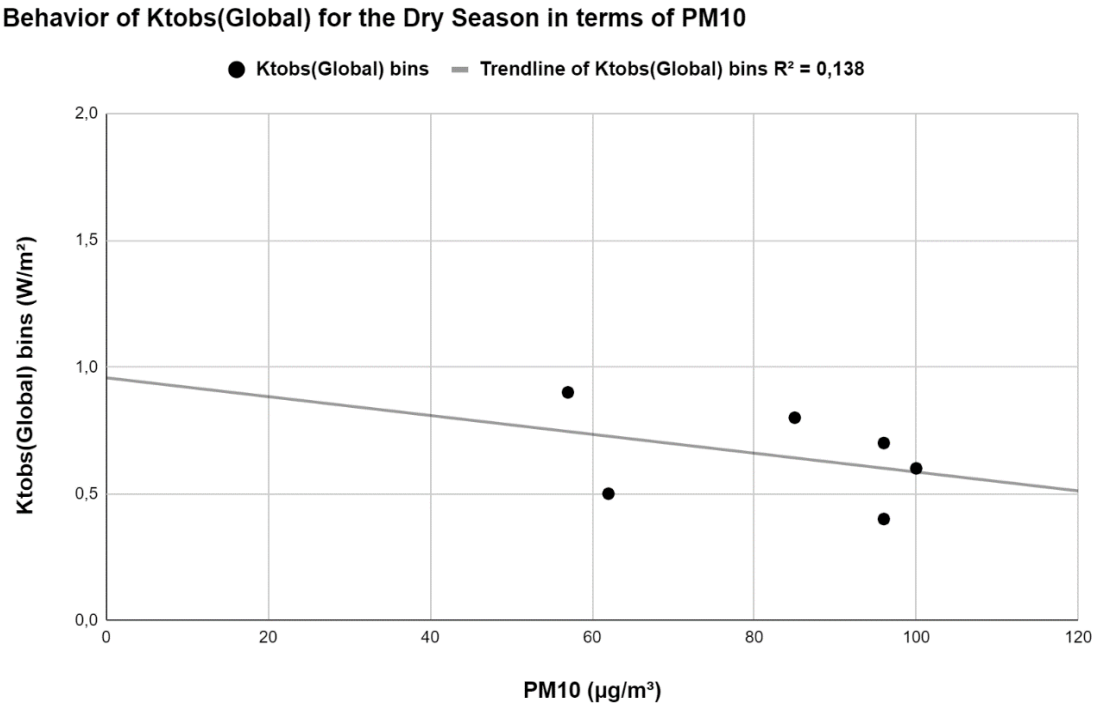

Source: By Author.

Table 4.2 – Ktobs (Global) bins related to maximum PM10 concentration in rainy and dry season.

Ktobs(Global) bins (W/m²)	PM10 concentration in rainy season (µg/m³)	PM10 concentration in dry season (µg/m³)
0.4	65	96
0.5	54	62
0.6	60	100
0.7	63	96
0.8	46	85
0.9	44	57
1	28	-

Source: By Author.

Figures 4.4 and 4.5 describe the correlation of global clarity index Ktobs (Global) and PM2.5 concentration for rainy and dry seasons, respectively. The plots are based on data from Table 4.3.

Once again, both figures show that the amount of solar global radiation reaching the Earth's surface decreases with the increase in PM2.5. However, for the rainy season, the correlation is $R^2 = 0.33$ and for dry seasons is $R^2 = 0.06$. This may be due to the specific characteristics of PM2.5 that will require a more detailed investigation.

Figure 4.4 - Behavior of Ktobs(Global) for the Rainy Season in terms of PM 2.5

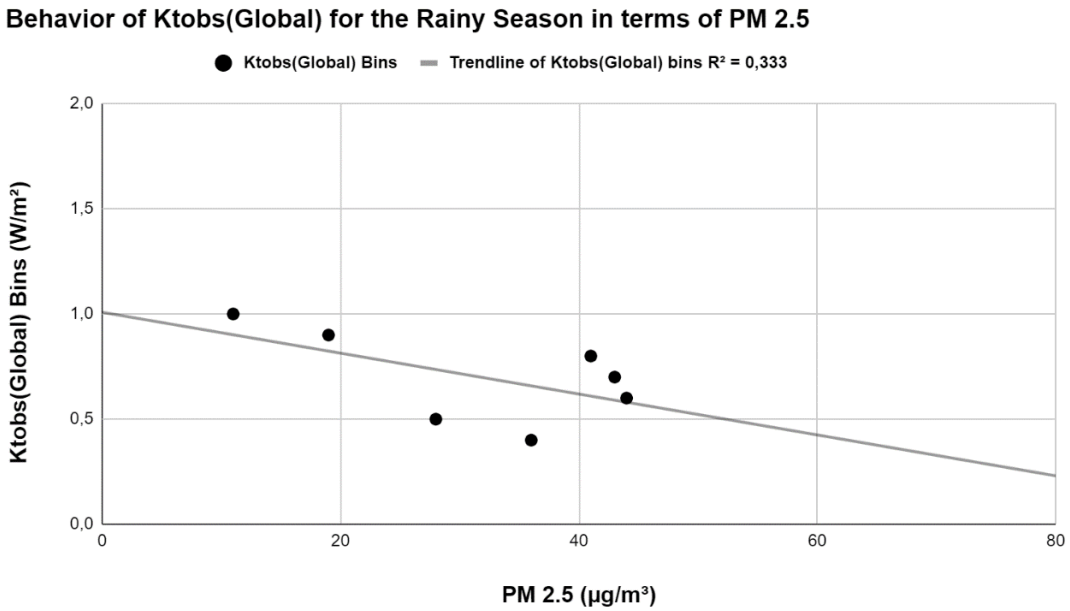

Source: By Author.

Figure 4.5 - Behavior of Ktobs(Global) for the Dry Season in terms of PM 2.5.

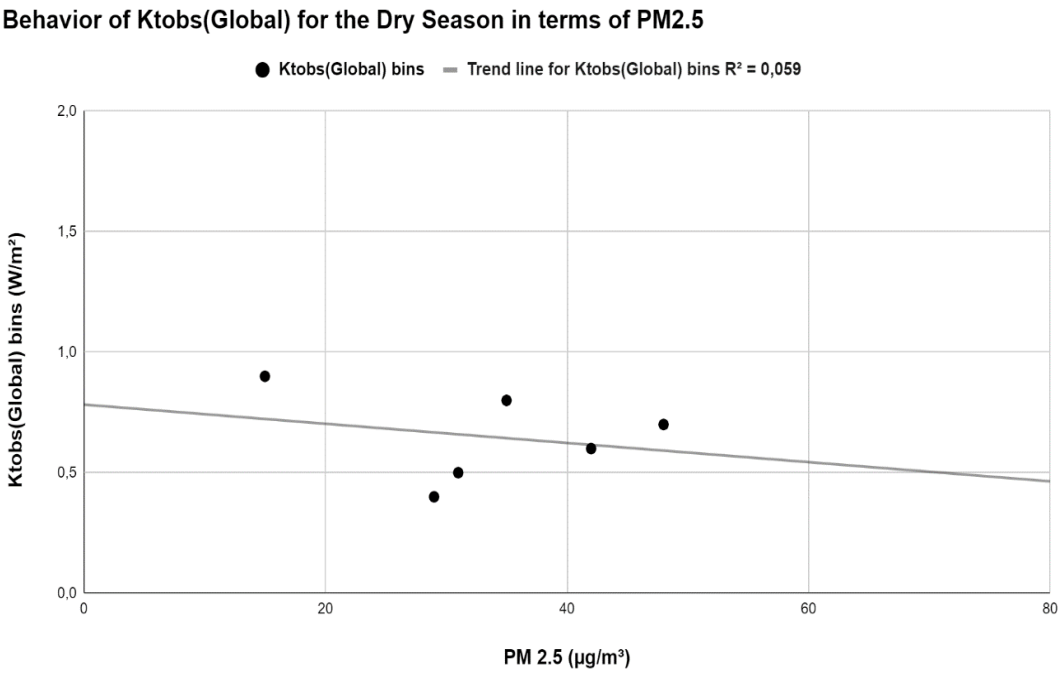

Source: By Author.

Table 4.3 – Ktobs(Global) bins related to maximum PM 2.5 concentration in rainy and dry season.

Ktobs(Global) bins (W/m²)	PM 2.5 concentration in rainy season (µg/m³)	MP2.5 concentration in dry season µg/m³
0.4	36	29
0.5	28	31
0.6	44	42
0.7	43	48
0.8	41	35
0.9	19	15
1	11	.

Source: By Author.

4.3 – Relation of the Ktobs(Global) and the Boomerang effect

Figure 4.6 shows the correlation of the BrasilDAT TL activity, the Ktobs(Global) index and the PM10 concentrations. As the PM10 concentration increases, the global solar radiation that reaches the ground decreases continuously. However, the lightning activity increases up to a particular level and then decreases.

Figure 4.6 - Behavior of the Boomerang Effect and Global Radiation (KTobs) for the rainy season.

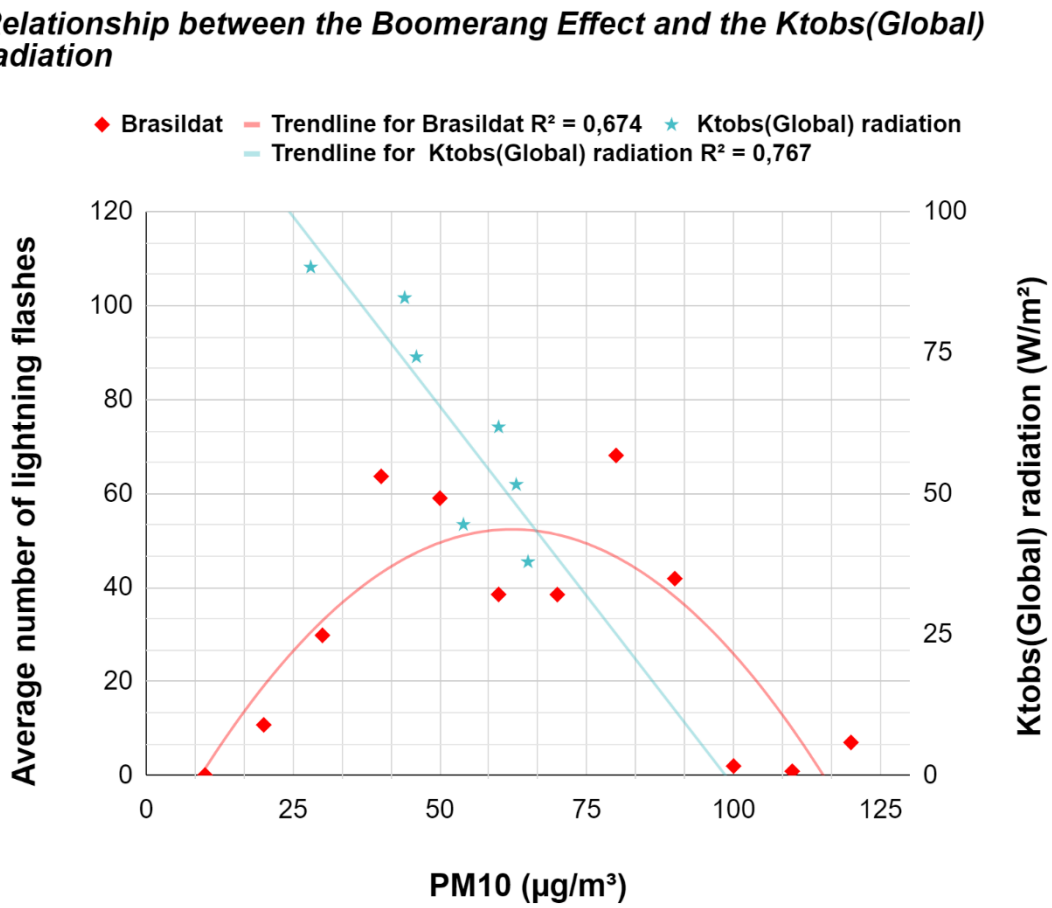

Source: By Author.

5 - CONCLUSIONS

5.1 – Boomerang effect in MRSP

The observed shape, referred to as the boomerang effect, is consistent with the findings of Koren et al. (2008) and Altaratz et al. (2010) for the Amazon region. Although, the aerosol characteristics in MRSP differs from the Amazon Forest, the effect of the aerosol concentration on lightning activity is similar. The boomerang shape in MRSP was first published by Farias et al. (2014).

When the concentration of PM10 increases, there is a corresponding increase in the number of lightning events, but as the aerosol concentration continues rising, at a particular level, the number of lightning events starts to decrease. This behavior results in a boomerang trend, which describes the initial increase of lightning activity followed by a decrease as the aerosols concentration monotonically increases.

These results and the findings of Koren et al. (2008), Altaratz et al. (2010) and Farias et al. (2014) show a consistency of the effect for different geographical locations and distinct aerosol characteristics. Thus, the processes governing the relation between aerosol concentration and lightning activity might be the same even if the environment are distinct. The similarity of findings over the Amazon Forest and the MRSP suggests a relevance of the Boomerang effect in driving the complex interactions between aerosols and lightning activity in diverse atmospheric environments. Therefore, studies are needed in different locations and with different types of aerosols to find a better understanding of the complexity between aerosol and lightning activity.

5.2 – Ktobs(Global) clarity index

The present work compared atmospheric PM2.5 and PM10 concentrations to global shortwave solar radiation trying to assess their interactions under the conditions of this work. In rainy season, PM10 had backscattered the incoming radiation pretty well, since the Ktobs(Global) decreased as the PM10 concentration increased with a high correlation. On the other hand, the correlation of the PM2.5 and the Ktobs(Global) is lower even for the rainy season. In the dry

season, there is a low correlation of the Ktobs(Global) and the PM10 and PM2.5 concentrations. One possible reason is the position of the Sun, which reduces the amount of global radiation that reaches the ground from April to September. In this case, since les radiation is crossing the atmosphere, less is the effect of the aerosol on it. Another reason is the less lightning activity during that period, which reduces the number of days with thunderstorms. Less days of data will affect the statistics leading to worse correlations. Finally, it was observed that PM2.5 presented a much less effect in reducing the global shortwave solar radiation that reaches the Earth's surface (which is essentially the Whitehouse effect) in comparison to the PM10. This is an interesting result showing that the PM2.5 does not contribute significantly to the Whitehouse effect as the PM10, which was able to effectively reduce the global radiation. Based on this fact, the PM10 tends to be the main responsible for the Whitehouse effect, which cools down the low levels of the troposphere.

5.3 - Relation of ktobs(Global) and the boomerang effect

Correlating the Ktobs(Global) clarity index, PM10 concentration and the number of lightning events (Figure 4.6), it was observed that the reduction of the global shortwave solar radiation that reaches the Earth's surface is very close connected to the boomerang effect of the lightning activity. The incoming radiation is maximum for PM10 concentrations below 30 μg/m³. As PM10 concentrations increase, the radiation decreases monotonically. On the other hand, the average number of lightning events increases in a parabolic way. When PM10 concentration reaches around 60 μg/m³, the amount of the incoming radiation continues to decrease while the lightning activity reaches its maximum and then starts to decrease. At that turning point, the Ktobs(Global) index is less than 50%, which means that a significative amount of radiation is being backscattered or absorbed by the aerosols. This is evidence that the Whitehouse effect might be in fact reducing the amount of heat available for convection, thus suppressing the thunderstorm formation and consequently reducing the lightning activity. However, this hypothesis requires further observations and analyzes to be confirmed because it is still not possible to assure that the reduction of the

Ktobs(Global) is in fact stabilizing the atmosphere by reducing the available energy for cloud amount.

6 - FUTURE RESEARCH

Interesting questions arise regarding how the Whitehouse effect can explain Boomerang effect:

1. Can the Whitehouse effect actually lead to atmosphere's stabilization? Is it possible to quantify this process?
2. Does this Whitehouse effect occur only in urban environments?
3. Which aerosol species are more efficient in backscattering and absorbing the shortwave incoming solar radiation?
4. Is the thunderstorm's microphysics affected by the Whitehouse effect? Does it change the electrification processes and consequently the polarity of the lightning events?
5. Is the Whitehouse effect significant enough to equalize the greenhouse effect?

Based on those questions, there are some possible future steps of this study

1. Verify whether the cooling down effect is in fact able to stabilize the atmosphere by analyzing altitude measurements that might show changes in the CAPE (Convective Available Potential Energy) and/or the atmospheric conditional instability.
2. Apply the same methodology to assess the Whitehouse effect in the Amazon region, where most of the aerosol are emitted or produced by natural sources instead human activities.
3. Analyze how other aerosols species (sulfates, nitrates, ozone, etc) and sizes interact with the shortwave incoming solar radiation in the atmosphere. This will help evaluate what type of aerosol are more effective in producing the Whitehouse effect.
4. Evaluate if the Whitehouse effect impacts in the thunderstorm's microphysics, affecting the electrification processes and thus changing the polarity and the intensity of the observed lightning events.

REFERENCES

AHRENS, C. D. **Meteorology today**. 9.ed. United States: Brooks/Cole, 2008.

ALTARATZ, O.; KOREN, I.; YAIR, Y.; PRICE, C. Lightning response to smoke from Amazonian fires. **Geophysical Research Letters**, v.37, n.7, Apr. 2010.

AMARANANWATANA, P.; CHUMNONG, S. An assessment of the ASHRAE clear sky model for irradiance prediction in Thailand Nuntiya. **Asian Journal on Energy and Environment,** v. 8, n. 2, p. 523-532, 2007.

ASHRAE handbook of fundamentals. Atlanta, Georgia: American Society of Heating, Refrigeration, and Air-Conditioning Engineers, 1985.

COMPANHIA AMBIENTAL DO ESTADO DE SÃO PAULO (CETESB). **Qualidade do ar no Estado de São Paulo**. São Paulo: CETESB, 2023. 162 p. Available in: <https://cetesb.sp.gov.br/ar/publicacoes-relatorios/>. Access in: 22 jan. de 2023.

COMPANHIA AMBIENTAL DO ESTADO DE SÃO PAULO (CETESB). **Qualidade do ar - dados horários.** 2023. Available from: https://cetesb.sp.gov.br/ar/dados-horarios/. Access in: 22 Jan. 2023.

CHARLSON, R. J.; LANGNER, J.; RODHE, H.; LEOVY, C. B.; WARREN, S. G. Perturbation of the Northern hemisphere radiative balance by backscattering from anthrpogenic aerosol. **Tellus**, v. 43, p. 52-163, 1991.

COORAY, V. **An introduction to lightning**. Berlin: Springer, 2015. 401p. ISBN: 978-9401789370.

DIVISÃO DE SATELITES E SISTEMAS AMBIENTAIS (DSA). **Banco de dados de Imagens**. 2023. Available from: https://satelite.cptec.inpe.br/acervo/goes16.formulario.logic. Access in: Feb. 2023.

FARIAS, W.R.G.; PINTO JUNIOR, O.; PINTO, I.R.C.D.A.; NACCARATO, K.P. The influence of urban effect on lightning activity: evidence of weekly cycle. **Atmospheric Research**, v. 135, p. 370–373, 2014**.**

GELENCSÉR, A. **Carbonaceous aerosol**: atmospheric and oceanographic sciences library. Berlin: Springer, 2005. 352 p. ISBN: 978-1402028861

GOODMAN, S. J. et al. The goes-r geostationary lightning mapper (GLM). **Atmospheric Research,** v.125, p. 34-49, 2013.

HINDS, W.C. **Aerosol technology:** properties, behavior and measurement of Airborne Particles. 2.ed. [S.l.]: Wiley, 2012. 504 p. ISBN: 978-1-118-59197-0.

HOBBS, P. V. **Aerosol-cloud-climate interactions**. San Diego: Academic Press, 1993. 235 p. ISBN: 978-0123507259.

HOUZE JUNIOR, R. A. **Cloud dynamics**. 2.ed. [S.l.]: Academic Press, 2014. 496 p.

INSTITUTO BRASILEIRO DE GEOGRAFIA E ESTATÍSTICA (IBGE). **Prévia da população dos municípios com base nos dados do Censo Demográfico 2022 coletados até 25/12/2022**. Rio de Janeiro: IBGE, 2023. Available from: https://www.ibge.gov.br/estatisticas/sociais/rendimento-despesa-e-consumo/22827-censodemografico-2022.html. Access in: Feb. 2024.

IQBAL, M, **An introduction to solar radiation**. [S.l.]: Academic Press, 1983. ISBN: 9780323151818.

JAMIL, B.; KHAN, M. Estimation of clear-sky solar radiation using ASHRAE model for Aligarh, India. **International Journal of Engineering Research and Technology.** v 7, n. 3, p. 227-236, 2014.

JOHNSON, T. M. et al. **Tools for improving air quality management:** a review of top-down source apportionment techniques and their application in developing countries. [S.l.]: ESMAP, 2011.

KOREN, I.; MARTINS, J. V.; REMER, L. A.; AFARGAN, H. Smoke invigoration versus inhibition of clouds over the Amazon. **Science,** v. 321, n. 5891, p. 946-949, 2008.

LIOU, K. N. **An introduction to atmospheric radiation**. 2.ed. [S.l.]: Academic Press, 2002. 608 p. ISBN: 9780080491677.

MOON. P. Proposed standard solar radiation curves for engineering use. **Journal of the Franklin Institute**, v. 230, n. 5, p. 583-617, 1940.

NACCARATO, K. P.; PINTO JUNIOR, O.; PINTO, I.R.C.A. Evidence of thermal and aerosol effects on the cloud-to-ground lightning density and polarity over large urban areas of Southeastern Brazil. **Geophysical Research Letters**, v. 30, n. 13, 2003.

PETTY, G. W. **A first course in atmospheric radiation**. 2.ed. [S.l.]: Sundog, 2006. 472 p. ISBN: 978-0972903318

REIST, P. C. **Aerosol science and technology**. 2.ed. [S.l.]: McGraw-Hill Education, 1993. 393 p. ISBN: 978-0071128490.

ROSENFELD, D. et.al. Flood or drought: how do aerosols affect precipitation? **Science**, v.321, n. 5894, p. 1309-1313, 2008.

ROSENFELD, D.; WOODLEY, W. Pollution and clouds. **Physics World**, v. 14, n. 2, p. 33-37, Feb. 2001.

SÃO PAULO. PREFEITURA MUNICIPAL. **Plano metropolitano RMSP análise territorial – subsídio ao macrozoneamento.** São Paulo: Prefeitura de São Paulo, 2016. 42p. Available from: https://gestaourbana.prefeitura.sp.gov.br/wp-content/uploads/2016/06/PDUI-mapas-alta-resolu%C3%A7%C3%A3o-parte-1.pdf. Access in: 23 Feb. 2024.

SAUNDERS, C. P. R. Thunderstorm electrification. In: VOLLAND, H. (Ed.). **Handbook of atmospheric electrodynamics**. 2.ed. Boca Raton: CRC Press, 1995. p. 61-92.

SAUNDERS, C. P. R.; KEITH, W. D.; MITZEVA, R. P. The effect of liquid water on thunderstorm charging. **Journal of Geophysical Research**, v. 96, n.D6, p. 11007-11017, June 1991.

SCHWARTZ, S. E. The whitehouse effect-shortwave radiative forcing of climate by anthropogenic aerosols: an overview. **Journal of Aerosol Science**. v. 27, n. 3, p. 359-382, 1996.

SEINFELD, J.H.; PANDIS, S.N. **Atmospheric chemistry and physics**: from air pollution to climate change. 2.ed. New York: Wiley, 2016. 1120 p. ISBN: 9781118947401**.**

STEPHENSON D. G. **Tables of solar altitude and azimuth, intensity and solar heat gain tables**. Ottawa, Canada: ETDWEB, 1967.

STEWART, I. D.; MILLS, G; **The urban heat island**. Canada: Elsevier, 2021. 182 p. ISBN: 9780128156902.

STULL, R. B. **An introduction to boundary layer meteorology**. Berlin: Springer, 1988. 684 p. ISBN: 978-9027727695.

THRELKELD. J. L.; JORDAN, R. C. Direct solar radiation available on clear days. **Heating, Piping, and Air Conditioning**, v. 64, n. 12, 1958.

THRELKELD, J. L. Solar irradiation of surfaces on clear days. **ASHRAE Transactions**, v. 69, p. 24-36, 1963.

VAREJÃO-SILVA, M.A. **Meteorologia e climatologia.** Recife: [s.n.], 2006.

WILLIAMS, E. R. Meteorological aspects of thunderstorms. In: VOLLAND, H. (Ed.). **Handbook of atmospheric electrodynamics**. Boca Raton: CRC Press, 1995.

APPENDIX A

The following table shows 142 days where GLM and Brasildat detect lightning activity and the maximum concentration of PM10 for each day.

Table A.1 – The 142 days where GLM and BrasilDAT detect lightning activity and the maximum concentration of PM10 for each day.

Days	GLM	BrasilDat	BrasilDat (CG)	PM10
05/09/2019	7	9	5	27
06/09/2019	6	3	2	41
19/09/2019	415	211	26	120
24/09/2019	77	210	99	74
27/10/2019	1	0	0	60
03/11/2019	5	26	4	79
20/11/2019	2	1	0	59
21/11/2019	119	574	283	83
30/11/2019	82	61	25	74
26/12/2019	0	1	1	53
30/12/2019	73	341	136	44
31/12/2019	152	692	123	70
05/01/2020	46	96	38	31
07/01/2020	48	46	15	57
16/01/2020	355	3112	605	77
28/01/2020	297	982	146	86
29/01/2020	518	388	132	53
01/02/2020	805	3654	554	35
08/02/2020	411	1811	261	46
09/02/2020	222	929	101	37
16/02/2020	373	849	187	64
17/02/2020	769	3963	913	57
18/02/2020	1606	4304	1401	55
19/02/2020	630	4521	1054	50
20/02/2020	474	2578	702	45
25/02/2020	697	2929	674	43
02/03/2020	1	3	1	43
08/03/2020	1448	11254	1828	47
15/03/2020	879	1811	539	45

continue

Table A.1 - Continuation.

16/03/2020	1286	4057	2095	38
17/03/2020	27	36	10	48
18/03/2020	5	5	2	71
25/03/2020	1	0	0	37
29/03/2020	500	1325	240	35
02/04/2020	2	7	1	43
02/05/2020	30	45	6	90
09/06/2020	16	10	1	80
13/08/2020	36	60	34	93
30/09/2020	677	1428	99	65
20/10/2020	1208	2468	1036	53
26/11/2020	1138	3072	859	47
27/11/2020	287	1054	284	65
29/11/2020	667	785	174	40
30/11/2020	722	2143	812	40
01/12/2020	847	3082	1365	21
04/12/2020	10	55	39	32
08/12/2020	1291	1980	962	35
09/12/2020	5	16	1	58
10/12/2020	1	0	0	42
14/12/2020	4	3	2	9
16/12/2020	828	2020	756	60
17/12/2020	945	733	403	27
18/12/2020	3647	4582	1996	39
20/12/2020	225	438	158	46
21/12/2020	565	1006	420	35
28/12/2020	315	585	262	37
30/12/2020	15	4	0	32
03/01/2021	400	646	115	14
09/01/2021	63	137	63	27
13/01/2021	18	30	23	48
16/01/2021	91	101	36	24
18/01/2021	206	174	75	38
31/01/2021	11	20	10	42
02/02/2021	2030	4103	2590	45
03/02/2021	725	1533	743	61
10/02/2021	930	2880	1256	26
16/02/2021	756	182	41	32

continue

Table A.1 – Continuation.

21/02/2021	18	5	5	46
24/02/2021	1067	3958	2139	62
25/02/2021	1707	3701	1566	35
27/02/2021	616	1097	551	27
28/02/2021	1523	4483	1440	32
02/03/2021	446	1062	705	57
03/03/2021	584	1376	565	51
04/03/2021	160	280	84	40
08/03/2021	1074	1643	992	36
09/03/2021	1144	972	533	37
14/03/2021	536	497	224	41
15/03/2021	0	5	1	46
16/03/2021	4	9	6	58
26/03/2021	310	776	298	49
27/03/2021	59	151	98	48
28/03/2021	1942	4606	962	51
30/03/2021	3236	1408	454	33
19/04/2021	4	0	0	16
21/04/2021	3	2	1	22
26/04/2021	78	46	16	53
15/09/2021	8	0	0	52
16/09/2021	2	0	0	37
12/10/2021	524	576	213	31
26/10/2021	4	9	2	36
12/12/2021	83	62	7	69
22/12/2021	508	750	154	63
16/01/2022	1850	2135	606	53
17/01/2022	56	84	43	43
19/01/2022	2428	10266	3178	33
25/01/2022	37	76	36	66
26/01/2022	667	2383	529	73
27/01/2022	266	657	101	39
05/02/2022	9	13	9	23
17/02/2022	137	120	35	34
19/02/2022	103	211	46	44
20/02/2022	929	2362	556	33
21/02/2022	156	231	116	44
22/02/2022	400	1604	645	54

continue

Table A.1 - Conclusion.

23/02/2022	938	6504	2	83
27/02/2022	19	130	27	64
02/03/2022		1	1	53
03/03/2022	247	260	116	54
05/03/2022	1904	9314	1578	40
07/03/2022	753	5878	2287	51
08/03/2022	303	1114	349	53
09/03/2022	441	1858	443	69
10/03/2022	171	368	152	46
12/03/2022	161	521	97	32
15/03/2022	243	642	241	42
16/03/2022	1314	5353	1047	44
18/03/2022	306	1169	349	65
26/03/2022	35	24	5	57
30/03/2022	0	2	2	46
04/04/2022	94	53	25	57
08/04/2022	267	381	162	55
19/04/2022	1	1	0	56
05/08/2022	11	4	3	104
12/09/2022	11	8	2	52
27/10/2022	154	186	15	86
28/10/2022	49	50	2	113
30/10/2022	24	24	1	65
20/11/2022	808	10546	773	72
26/11/2022	129	666	45	35
09/12/2022	5	39	4	86
11/12/2022	490	2542	549	68
16/12/2022	67	111	21	63
24/12/2022	98	468	149	83
02/01/2023	440	1016	254	49
17/01/2023	1318	8136	2427	46
18/01/2023	78	606	93	51
19/01/2023	919	4931	2171	42
29/01/2023	1107	6264	941	34
09/02/2023	991	2251	387	61
20/02/2023	0	3075	662	46
27/02/2023	0	150	37	31

Source: By Author.